COMPRESSIBILITY BEHAVIOR OF BENTONITES BY STERN THEORY BASED ON CONSTANT SURFACE CHARGE CONDITIONS

[1]DHANESH SING DAS

Assistant Professor,

[2]TADIKONDA VENKATA BHARAT*

Professor,

[3]SURESH RAJA

Associate Consultant,

[4]SNEHASIS TRIPATHY

Professor,

[1]Department of Civil Engineering, National Institute of Technology Goa,
Farmagudi, Ponda – 403401, Goa, India

[2]Department of Civil Engineering, Indian Institute of Technology Guwahati,
Guwahati – 781039, Assam, India

[2]Data Science and AI, KMPG Global Service, Eco world, Campus 7, Devarabeesanahalli,
Marathalli Outer Ring Road, Bengaluru– 560103, Karnataka, India

[3]Cardiff School of Engineering, Cardiff University,
Queens Buildings, West Groove, Newport Road, Cardiff CF243AA, UK

*Corresponding Author, Email: tvb@iitg.ac.in

ABSTRACT

The compressibility behavior of clays is governed by the electrical double layer formed around the clay particles. The Gouy-Chapman diffuse double layer theory is often utilized to predict the compressibility behavior of clays. The theory, however, does not consider the effect of the size of the cations and thus predicts unrealistically small void ratios for compacted bentonites under large mechanical pressures expected in high-level nuclear waste repository applications. In this study, the Stern layer was introduced to incorporate the cations size effect in the prediction of the compressibility behavior of bentonites. The overall diffuse double-layer thickness at large pressures was found to be much smaller than the initially assumed Stern layer thickness based on the exchangeable cation size for all the studied bentonites. A compressible Stern layer was, therefore, considered for the first time in the prediction of the compressibility behavior of bentonites. The compression behavior of the Stern layer under the applied loading is influenced by the ratio of the mid-plane to the Stern potential, which is dependent on the type and composition of the exchangeable cations on the clay surface. Stern layer compression was initiated when the potential ratio is in the range of 0.65-0.75 for bentonites with different surface cations characteristics. The incorporation of cation size and compressible Stern layer provided significant improvements over the existing models in predicting the compressibility behavior of bentonites over a wide pressure range. The predicted compressibility data by the proposed model showed a very good agreement with the measured data of five different bentonites from the literature in the pressure range of 0.1-42 MPa.

Keywords: Bentonites, compressibility behavior, cation size effect, diffuse double layer theory

INTRODUCTION

Bentonites are predominantly comprised of the expansive smectite group of minerals and exhibit attractive features such as high ion adsorption capacity, high swelling capacity, and very low hydraulic conductivity (Benson et al., 1994; Glatstein and Francisca, 2015; Kaufhold et al., 2015; Chen et al., 2016). Bentonites are widely used in various Geotechnical and Geoenvironmental engineering field applications. Compacted bentonites have been considered as buffer and backfill materials for underground high-level nuclear waste repository systems in many countries (Butcher & Mu¨ller-Vonmoos, 1989; Ishikawa et al., 1990; Japan Nuclear Cycle Development Institute, 1999; ENRESA, 2000; Tripathy et al., 2004; Bharat et al., 2013; Pusch, 2015; Zheng et al., 2017). These facilities are being planned at a depth of ~ 500 to 1000 m below the ground level in different countries (Atomic Energy of Canada Limited (AECL), 2002; Enviros, 2003). The geostatic stress at such depth is expected to be in the range of 9 to 40 MPa (Tripathy & Schanz, 2007). The magnitude of stress in landfill liners and tailing impoundments are usually expected to be in the range of 0.36 to 6 MPa (Peirce et al., 1986; Timmons et al., 2012). Several studies considered the stress range of 3 to 42 MPa for studying the compressibility behavior of bentonites in these applications (Baille et al., 2010; Marcial et al., 2002; Tripathy & Schanz, 2007; Pusch et al., 2011; Bharat et al., 2013; Ye et al., 2014). Laboratory estimation of compressibility behavior at high pressures, however, is highly time-consuming and expensive as it requires specialized heavy equipment and loading mechanisms (Ng et. al., 2006; Tripathy & Schanz, 2007).

Empirical models have been proposed in the past to predict the compressibility behavior of natural soils (Nagaraj & Srinivasa Murthy, 1986; Burland, 1990; Bharat & Sridharan, 2015). The applicability of these models, however, is limited to a certain range of soil plasticity and lower ranges of applied pressures. The Gouy-Chapman model for interacting parallel clay-water-ion

system has been used to predict the compressibility behavior of clays (Bolt, 1956; Sridharan & Jayadeva, 1982; Tripathy et al., 2007; Bharat & Sridharan, 2015). Discrepancies have been observed between theoretical predictions and the measured compressibility data primarily due to the assumption of the parallel arrangement of the clay platelets and the treatment of the cations as point charges in the theory (Bolt, 1956; Warkentin et al., 1957). Stern (1924) incorporated the effect of the size of cations by introducing a thin and compact layer of cations next to the clay platelet surfaces to the original Gouy-Chapman model DDL. The Stern model has been utilized to study the electrical potential distribution of non-interacting clay platelet systems (Verwey & Overbeek, 1948; van Olphen, 1977; Shang et al., 1994; Sridharan & Satyamurthy, 1996) and the compressibility behavior of bentonites based on the constant surface potential (CSP) condition (Tripathy et al., 2014). The Stern theory at constant surface charge condition (CSC) is, however, favored for the clays as their basal surfaces possess constant/permanent charges. Prediction of the clay compressibility behavior using the interacting Stern theory at CSC condition is not available so far as the mathematical formulation of electrostatic potential distribution remains to be established.

In this study, an improved predictive model was presented for the compressibility behavior of bentonites by considering the effect of the size of cations. The Stern DDL theory of CSC condition was utilized based on the postulation that clay platelets were in a parallel arrangement under high applied pressures. The Stern layer thickness, however, is still not well-defined for clays. Although, most of the available studies consider the Stern layer to be incompressible, in the present study it was shown based on the measured void ratios that the DDL thickness at large applied pressures is much smaller than the Stern layer thickness.

95 The proposed model, thus, incorporates the compressibility of the Stern layer thickness which
96 depends on the ratio of mid-plan to Stern potential as identified in this study. The measured
97 compressibility data of five different bentonites representing a wide range of surface area and
98 surface cations in the pressure range of 0.1– 42 MPa were considered from the literature to validate
99 the proposed model. The Gouy-Chapman model and the Stern model for CSP conditions were also
100 considered for the comparative assessment.

101 # DIFFUSE DOUBLE LAYER THEORY

102 The interaction of clays with water or other electrolytes is important in understanding the
103 engineering aspects of clays *viz*., the volume change behavior, chemical sorption, and flow-related
104 problems. Clay-water interaction involves physicochemical forces because of the electrochemical
105 activity of the clay surface. The Van der Waals (VdW) attractions, capillary interactions,
106 Coulombic attraction and repulsion, and long-ranged diffuse double-layer repulsive forces are the
107 important surface forces that are known to be existing in clays (Verwey and Overbeek, 1948; Bolt,
108 1956; Bishop, 1959; Lambe, 1960; Skempton, 1960; Sridharan and Rao, 1973; van Olphen, 1977,
109 Mitchell, 1993; Lu and Likos, 2006; Lamb and Whitman, 2008; Israelachvili 2011). While the
110 Coulombic forces are negligible in expansive clays dominated by montmorillonite minerals, the
111 capillary forces are absent at full saturation (Schubert 1975, Lu and Likos, 2006). The VdW forces
112 are significant at smaller inter-particle separation distances (Israelachvili, 2011), however, their
113 influence on the compressibility behavior is not well understood so far. The VdW forces may be
114 considered passive type forces during compression as they are compressive in nature and will
115 remain inactive during the compression loading. The magnitude of the VdW forces, however,
116 increases under the application of compressive stress due to the reduced separation distance or
117 enhanced particle-particle interaction. The increased VdW forces are activated during the stress

118 removal and significantly control the rebound or swelling response of the soil. The long-ranged
119 diffuse double layer (DDL) repulsive forces, on the other hand, are predominant in saturated
120 montmorillonite clays and primarily control the compressibility behavior (Bolt, 1956, Mitchell,
121 1960, Olson and Mesri, 1970, Sridharan and Rao, 1970, 1972). The Vdw forces are, thus, often
122 neglected and the compressibility behavior of clays is obtained based on the equilibrium between
123 the applied mechanical stress and the repulsive forces. The Gouy-Chapman DDL theory is
124 commonly used to understand the clay-water-electrolyte interaction, which relates the repulsive
125 forces to the electrostatic potential distribution in the clay-water system (Bolt,1956, Honig and
126 Mul, 1971, Komine and Ogata, 2003, Bharat et al., 2013, Bharat & Sridharan, 2015a & b). A brief
127 description of the diffuse double layer theory is presented below followed by the theoretical
128 formulation of the compressibility behavior.

129 Net negative charges are available on the basal surfaces of clay platelets (montmorillonite
130 minerals) due to the isomorphous substitution of Al^{3+} by Mg^{2+} in the crystal structure of the
131 octahedral alumina sheet (Grim, 1968; Mitchell & Soga, 2005). Exchangeable cations are naturally
132 present on the clay surface to compensate for the negative charges. In the presence of a
133 water/electrolyte medium, the cations on the clay surface experience an additional diffusive type
134 of force that tries to drive the cations away from the charged clay surface. The diffusive forces
135 are developed due to the existing concentration gradient of the cationic species between the clay
136 surface and the bulk electrolyte solution. An electric diffuse double layer (cation cloud) is formed
137 around the clay platelets as a consequence of the competition between the strong electrostatic
138 attraction between the cations and negatively charged clay surface, and the diffusive forces
139 (Verwey & Overbeek, 1948; Van Olphen, 1977; Sparks, 1999). The DDL around the clay platelet
140 primarily controls the interaction among the clay platelets and often leads to the parallel plate

orientation in the saturated clays. For such a parallel plate configuration, the DDL around the clay platelets defines the separation distance among the clay platelets which is related to the macroscopic void ratio. Thus, the compressibility behavior of clays is predicted by the theoretical estimation of the thickness of the DDL around clay platelets (Bolt, 1956, Sridharan & Jayadeva, 1982, Sridharan & Choudhury, 2002, Tripathy et al. 2007).

An illustration of the interacting parallel-plate clay-water-electrolyte system under applied mechanical pressure by the Gouy-Chapman DDL model (Gouy, 1911; Chapman, 1913) is presented in Fig.1. As the two clay platelets approach each other under the action of applied mechanical stress, repulsive pressure (P_R) develops between the clay platelets due to the interaction of the similarly charged DDL around the clay platelets. The separation distance between two neighboring clay platelets continues to decrease under the applied mechanical stress until it reaches an equilibrium state. Under this condition, the repulsive pressure is equal to the applied mechanical pressure (P) on the system (Bharat & Sridharan, 2015a; Bharat & Das, 2017). The electrostatic potential distribution within the interacting system is represented by the curve y(x) with a minimum potential (u) at the mid-plane as shown in Fig. 1. The midplane potential is related to the repulsive pressure between the two platelets or the applied mechanical pressure at equilibrium as per the equation given by Langmuir (1938) presented below (van Olphen, 1977; Mitchell & Soga, 2005),

$$P_R = P = 2nkT\left(\cosh\left(u\right)-1\right) \quad (1)$$

where n is the concentration of cations in the electrolyte solution in ions/m^3, k is the Boltzmann constant ($=1.38\times10^{-23} J/K$), and T is the temperature in K. The mid-plane potential is uniquely related to the separation distance between the clay platelets and represents the degree of interaction

in the system. The relationship between the mid-plane potential and the separation distance is given by the Poisson-Boltzmann's equation as (van Olphen, 1977)

$$t_{DDL} = -\frac{1}{\kappa}\int_{y_0}^{u} (2\cosh(y) - 2\cosh(u))^{-1/2} dy \quad (2)$$

where, t_{DDL} is the DDL thickness, which is equal to half of the separation distance (d) in the Gouy-Chapman DDL model, $\frac{1}{\kappa}$ ($\kappa = \sqrt{\frac{8\pi q^2 v^2 n}{\varepsilon D_0 kT}}$) is the Debye length (Verwey & Overbeek, 1948; van Olphen, 1977; Bharat & Sridharan, 2015b), q is the electronic charge ($=1.6\times10^{-19} C$), v is the valence, ε is the dielectric constant, D_0 is the dielectric permittivity of vacuum ($=8.854\times10^{-12} C^2/N-m^2$), y_0 is the normalized electrostatic potential at the clay surface. The surface potential estimated for a given soil surface and electrolyte properties given by

$$\left(\frac{dy}{d\xi}\right)_{x=0} = \sqrt{2\cosh(y_0) - 2\cosh(u)} = \sigma\sqrt{\frac{1}{2\varepsilon D_0 nkT}} = 0.96352\frac{C_e}{S_a}\sqrt{\frac{1}{2\varepsilon D_0 nkT}} \quad (3)$$

where $\left(\frac{dy}{d\xi}\right)_{x=0}$ is the slope of the potential distribution curve near the clay surface, σ is the total surface charge density on the clay surface, C_e is the cation exchange capacity in meq/100g, and S_a is the specific surface area in m^2/g. The macroscopic void ratio is related to the inter-platelet separation distance as per the following equation (Bolt, 1956; Bharat & Das, 2017),

$$e = G\rho_w S_a \, d/2 \quad (4)$$

where, $d/2$ is the half of the separation distance between two parallel clay platelets, G is the specific gravity. The void ratio at any given pressure, thus, can be estimated using Eq. 1-3

assuming a parallel plate orientation of the clay platelets. The integral involved in Eq. 2 is elliptic, which is to be solved numerically to establish the relationship between mid-plane potential and separation distance (Bharat et al., 2013).

Stern DDL theory

The finite size of the cations at the particle surface limits the closest approachable distance to the charged clay surface (Stern, 1924). This results in a relatively compact and immobile layer of counter-ions close to the surface, which is followed by a diffused layer of the counter-ions. Thus the electric double layer in a clay-water system is characterized by the Stern layer and the outer diffused layer consisting of the Gouy layer. The center of the spherical cations in the Stern layer is at a distance of approximately equal to their hydrated radius away from the clay surface (Guven & Pollastro, 1992), which is defined as the outer surface of the Stern layer (Shang et al., 1994). The charge within the Stern layer is constant and the electrostatic potential varies linearly from a maximum value (y_0) at the clay surface to y_δ at a distance equal to the Stern thickness (δ) at the Stern-Gouy interface where the potential is termed the Stern potential. The dielectric constant of water within the Stern layer is significantly reduced to 3-6 as the water molecules are tightly bound to the clay surface (Verwey & Overbeek, 1955; Sridharan, 1962; van Olphen, 1977; Sposito, 1984; Hunter, 1987; Shang et al., 1994; Sridharan & Satyamurty, 1996). A graphical illustration of the Stern model for the interacting clay-water system is presented in Figure 2. The inter-platelet separation distance, *d,* in the Stern model is the summation of the Stern layer thickness δ and the thickness of the Gouy diffuse layer, t_{DDL}.

$$d = 2(\delta + t_{DDL}) \tag{5}$$

201 The electrostatic potential distribution within the Stern layer is dependent on the surface charge
202 density and the dielectric properties of the pore fluid as given in Eq. (6)

203 $$\sigma = \frac{\varepsilon' kT}{4\pi\delta vq}\left(y_0 - y_\delta\right) \quad (6)$$

204 Within the Gouy layer, the electrostatic potential distribution varies non-linearly between Stern
205 potential (y_δ) at the x = δ and mid-plane potential (y_d) at x = *d/2*, which is represented by the
206 Poisson-Boltzmann equation:

207 $$\kappa t_{DDL} = -\int_{t_{DDL}-\delta}^{t_{DDL}} d\xi = -\int_{y_\delta}^{u} (2\cosh(y) - 2\cosh(u))^{-1/2}\, dy \quad (7)$$

208 Evaluation of the Stern potential (y_δ) is prerequisite for the estimation of Gouy layer thickness
209 (t_{DDL}). The relationship between the charge density and potential distribution is utilized to
210 determine the Stern potential for a given clay-water-electrolyte system. The Stern layer charge (σ_1)
211 and Gouy layer charge (σ_2) together balance the total negative surface charge (σ) on the clay
212 platelets:

213 $$\sigma = -(\sigma_1 + \sigma_2) \quad (8)$$

214 The clay platelets are treated as constant-charged plates (Grim 1968), for which the total surface
215 charge density can be expressed as,

216 $$\sigma = 0.96352\frac{C_e}{S_a}\ \text{C/m}^2$$

where C_e is the cation exchange capacity of soil expressed in *meq*/100*g* and S_a is the specific surface area expressed in m^2/g. The charge density in the Stern layer can be obtained as (Verwey & Overbeek, 1948);

$$\sigma_1 = \frac{N_1 vq}{1+\left(N_A/Mn\right)\exp\left(-\left(y_\delta + {\psi vq}/{kT}\right)\right)} \tag{9}$$

where N_1 = no. of adsorption spot per 1 cm^2 area of the clay surface, v is the valence of ions, N_A = Avogadro's number, M = molecular weight of the solvent (water), y_δ = Stern potential at the plan separating Stern and Gouy layer, ψ = specific adsorption potential on the counter-ions at the surface. The charge in the Gouy layer can be derived as (Verwey and Overbeek, 1948; van Olphen, 1977);

$$\sigma_2 = \sqrt{2nkT\varepsilon}\sqrt{2\cosh y_\delta - 2\cosh u} \tag{10}$$

Combining Eqs. 6 and 8-10, the Stern potential can be expressed as a function of the mid-plane potential and the pore fluid parameters, which in turn can be used along with Eqs. 1 and 6 to estimate the void ratio at a given pressure. Equation (9) is only valid for non-interacting systems (van Olphen, 1973) and requires modification for applying to the interacting clay-water system. The number of available spots in the bulk solution, N_1 is dependent on the volume of the diffuse layer which is subjected to change with the change in the degree of interaction under the applied pressure. van Olphen (1973) presented the following equation to replace Eq. 9 for an interacting system,

$$\sigma_1/\sigma_2 = \left[\delta\Big/\left(\frac{d}{2}-\delta\right)\right]\exp\left[y_\delta + \left(\psi/kT\right)\right] \tag{11}$$

236 The inter-particle distance can be estimated from Eq. 12,

237 $$\kappa t_{DDL} = -\int_{\delta}^{d/2} d\xi = -\int_{y_\delta}^{u} (2\cosh(y) - 2\cosh(u))^{-1/2} dy \quad (12)$$

238 Eq. 11 is derived based on the assumption that statistical charge distribution between the Stern and
239 Gouy layer is proportional to their respective volumes or their respective thickness. The equation,
240 however, leads to erroneous estimation of electrostatic potential distribution as it does not utilize
241 the correct volume of the Gouy diffused layer.

242 The interacting Stern model is utilized for predicting the compressibility behavior of clays by
243 assuming the clay surface potential to be constant (Tripathy et al., 2014). Since montmorillonites
244 possess constant surface charge (Grim, 1968), the assumption of constant surface potential may
245 not be tenable. Therefore, estimation of Stern potential and DDL thickness requires modification
246 of the Stern theory, which has been dealt with in this study.

247 ## STERN-GOUY MODEL FOR CONSTANT SURFACE CHARGE

248 van Olphen (1963) suggested that the charges in the Stern and Gouy layers can be proportional to
249 their respective areas under the electrostatic potential distribution curve (Eq. 14).

250 $$\frac{\sigma_1}{\sigma_2} = \frac{\text{Area of the Stern layer } (A_s)}{\text{Area of Gouy layer } (A_{Gouy})} \quad (14)$$

251 The estimation of Stern layer charge (σ_1) in an interacting system for CSC conditions is not
252 available due to the difficulties involved in estimating the two parameters, such as the number of
253 available adsorption sites and specific adsorption potential on the counter-ions at the clay surface
254 (see Eq. 9). The influence of platelet interaction on the number of available adsorption sites is not

understood yet. Further, the specific adsorption potential, ψ for a given clay-water-electrolyte system is difficult to estimate under varying DDL interaction. In this study, estimation of σ_1 was eliminated and the following equation was developed to determine the Stern potential at a given pressure by knowing the soil surface and pore-fluid properties. (*Detail derivation is presented in the Appendix*)

$$\sigma A_{Gouy} = \sqrt{2nkT\varepsilon}\sqrt{2\cosh y_\delta - 2\cosh u}\left(\left(y_\delta + \left(vq\sigma 2\pi\delta/\varepsilon' kT\right)\right)\delta + A_{Gouy}\right) \quad (15)$$

The area under the hyperbolic potential distribution curve for the Gouy layer (A_{Gouy}) is a function of Stern and mid-plan potentials which can be calculated by following the method of slices (See Appendix). Therefore, Eq. (15) provides an implicit solution for the Stern potential. For a known value of mid-plan potential, Stern potential is obtained through optimization. The objective function to determine the Stern potential based on Eq. (16) is given as,

$$f\left(y_\delta\right) = \sigma A_{Gouy} - \left\{\sqrt{2nkT\varepsilon}\sqrt{2\cosh y_\delta - 2\cosh u}\left(\left(y_\delta + \left(vq\sigma 2\pi\delta/\varepsilon' kT\right)\right)\delta + A_{Gouy}\right)\right\} \quad (16)$$

The 'fminbnd' function, which is based on the golden section search and parabolic interpolation method, was used to obtain the optimized value of Stern potential from the objective function (Eq. 16) in Matlab. The mid-plane potential, *u*, was used as the lower boundary in the optimization, added a small value (~ 10^{-9}) to avoid the singularity (Bharat et al., 2013). The upper boundary was fixed at 30 for the studied pressures and pore fluid concentrations. The nature of the objective function was, further, studied at three different applied pressures and four different pore fluid concentrations. The important parameters used in the objective function evaluation are presented in Table 1. For all the cases, the true minima are preceded by a minimum at the lower boundary (i.e., *u*). The true minima approach the first minima (*u*) with the increase in the applied

pressure (Fig. 3a) and pore fluid concentration (Fig. 3b). Overall, the local minimum was observed in the range of 0−10 for all the considered cases.

Electrostatic potential distribution

The potential distribution for the entire DDL in the Gouy-Chapman model follows the Poisson's distribution from a maximum value at surface to a minimum at the mid-plane. In the case of Stern model, the potential starts with a maximum value at the surface, and reduce linearly to Stern potential at the Stern-Gouy interface. Beyond this, the potential follows the Poisson's distribution within the Gouy-layer to a minimum value at the mid-plane. The mid-plan potential u, at a given pressure was determined using Eq. 1. The surface potential was obtained using Eq. 3 for the Gouy-Chapman model and Eq. 6 for the Stern model after knowing the Stern potential. The Stern potential was estimated through optimization using Eq. 22 for known u.

Fig. 4a presents the potential distributions for both models from the surface to mid-plane distance under two different applied pressure at equilibrium. The parameters considered in the computation are presented in Table 1. At the lower applied pressure (0.01 MPa), the influence of the size of the cations was only visible near the clay surface up to a distance of ~ 20 Å. At higher applied pressure, the effect of cations size on the potential distribution was more pronounced due to the increased DDL interaction as the separation distance reduced significantly.

Fig. 4b presents the variation of Stern potential, mid-plane potential, and the DDL thickness (on the third axis) of an interacting clay-water system with the applied pressure by the proposed Stern model. The values of all parameters considered in the simulation were presented in Table 1. The applied pressure varied in the range of 0.01 MPa to 40 MPa. The DDL thickness decreased exponentially with the applied pressure and attained a minimum thickness of 7.9 Å (hydrated radius of Na^+ cation), equivalent to the Stern thickness at ~ 5 MPa. This indicated the full

compression of the diffused Gouy-layer leading to compact layers of cations around the clay platelets. The DDL thickness, thus, remained constant with a further increase in the pressure. The mid-plane potential linearly increased with the increase in the applied pressure on the semi-log scale due to the increased DDL interaction. The Stern potential, on the other hand, showed a relatively slower rise in magnitude as compared to the mid-plan potential. The two potential curves eventually converged beyond ~ 7-8 MPa pressure as the mid-plane coincided with the Stern boundary after the elimination of the Gouy-layer. The ratio between the Stern potential and the mid-plan potential, thus, is a useful parameter to understand the compressibility behavior of the DDL under the applied pressure.

Stern layer thickness at large pressure

Choosing an appropriate thickness of the Stern layer is crucial for predicting the pressure-void ratio relationship, especially in the higher-pressure range, where the Gouy diffused layer gets compressed significantly. The minimum possible void ratio (i.e., the minimum separation distance between two interacting clay platelets) in clays is controlled by the thickness of the Stern layer. A well-defined value for the Stern layer thickness, however, is not available for the clays (Verwey & Overbeek, 1948; van Olphen, 1973; Shang et al., 1994; Sridharan & Satyamurhty, 1996). The type of exchangeable cations, charge distribution, and size and shape of the siloxane cavity on the surface of the montmorillonite influence the adsorption of cations on the clay surface (Sposito, 2008), which can significantly influence the Stern layer thickness. Most of the available studies consider the Stern layer to be incompressible and equivalent to the radius of the hydrated cations, but the interaction between the particles considered in such studies is weak or negligible. The behavior of the Stern layer at large applied pressure, however, is not studied so far.

Experimentally determined compressibility data of seven different bentonites from the literature were considered in this study to understand the minimum achievable separation distance between the clay platelets (DDL thickness) under the applied mechanical pressures. The relevant properties of the bentonites are presented in Table 2. The DDL thickness was derived from the experimental void ratio for these bentonites from the literature using Eq. 4 by considering the parallel plate assumption. The void ratio of the bentonites considered in this study was in the range of ~0.4–1 under the studied pressure range. The parallel arrangement of the clay platelets has been well reported for heavily consolidated clays at such small void ratios (Delage & Lefebvre, 1984). Strong DDL repulsion brings the clay platelets towards a parallel arrangement as the soil is heavily compressed at large pressure. The DDL thickness was plotted against the applied pressure and presented in Fig. 5a. Variation of the DDL thickness with the applied pressure for all the bentonites suggested that the thickness of the DDL is compressed to the smallest value of 2.3 Å in the pressure range of 10 MPa- 40 MPa for different bentonites. The minimum possible separation distance between the two clay platelets surrounded by a rigid Stern layer is shown in Fig. 5b(i). When the DDL thickness or the half of the separation distance is decreased beyond the value equivalent to the diameter of the exchangeable cation, the Stern layer thickness consequently got compressed. The Stern layer compression is facilitated by the penetration of the surface cations into the siloxane cavities of the clay surface (Fig. 5b (ii)) once the diffuse layer is eliminated from the system at a large applied pressure. Generally, the diameter of the siloxane cavity is about 2.6 Å, which is approximately 1/3rd of the hydrated size of Na^+ (Sposito, 2008) and about similar in size as that of water molecules. The Stern layer, thus, get compressed at a high applied pressure to facilitate further volumetric compression of clays once the Gouy-layer is compressed significantly.

343 The total DDL thickness at large pressure was, therefore, corrected through the incorporation of
344 the Stern layer compression. The compressibility of the Stern layer was, however, incorporated
345 only into the void ratio computation in Eq. 4. The effect was not considered in the computation of
346 Stern potential and the thickness of the Gouy-layer, as the theoretical formulation for such a
347 complex interaction is not available. The ratio of mid-plan to Stern potential (u/y_δ) during the
348 compression of the DDL thickness under the applied pressure was studied for three different
349 bentonites namely Na-Kunigel, Ponza, and Na-Ca-MX80 (Fig. 6). The three bentonites
350 represented a wide range of surface cation characteristics and surface charge density (σ). The ratio
351 between the two potentials indicated the degree of interaction between the two interacting clay
352 platelets. The relevant properties of the respective bentonites and other parameters related to the
353 pore-fluid and Stern layer used in the estimation are presented in Table 2 & 3, respectively. A
354 cationic concentration of 0.0001N was used to represent water as pore fluid (Das & Bharat, 2021).
355 The Stern layer thickness was taken as the hydrated radius of Na^+ for Na-dominated bentonite. For
356 the divalent dominated and mixed-valence bentonites, the larger cationic size (i.e., Ca^{2+}) was
357 considered as the Stern layer thickness.

358 The potential ratio increased with the applied pressure for all the three bentonites as the DDL
359 thickness was compressed resulting in a higher degree of DDL interaction. The Stern layer
360 compression began when the potential ratio was ~ 0.65 for the di-valence-dominated Ponza
361 bentonite as well as the mixed-valent Na-Kunigel bentonite (Fig. 6a). On the other hand, Stern
362 layer compression was observed at ~ 0.75 for the Na-dominant Na-Ca-MX80 bentonite. The
363 observed difference in the potential ratio at the beginning of the Stern layer compression for
364 different bentonites was related to the variation in the surface cation characteristics and surface
365 charge density. Stern layer compression started early for the bentonites containing higher surface

charge densities and di-valent cations. Overall, the Stern layer compression begins when the potential ratio was in the range of 0.65-0.75 for different bentonites.

An S-curve relation between the Stern layer thickness (δ) and the ratio between the mid-plan and Stern potential was assumed to predict the void ratio, which follows the typical compressibility behavior of clays, as given by

$$\delta = r\exp^{-\left\{a\left(\frac{u}{y_\delta}-R_y\right)\right\}} \quad ;\frac{u}{y_\delta}-R_y>0 \tag{23}$$

where r is the hydrated radius of cation in Å, R_y is the potential ratio at which Stern layer thickness starts getting compressed, varies in the range of 0.65-0.75, depending on the surface charge characteristics of the clays. The parameter 'a' defines the slope of the curve, which was determined based on the observed minimum achievable thickness of the Stern layer (~2.3 Å) when the potential ratio becomes unity, as given by

$$a = (R_y - 1)\ln\left(\frac{2.3\,\text{Å}}{r}\right) \tag{24}$$

The above correction for Stern layer thickness was incorporated into the void ratio computation through Eq. 5 when the potential ratio reaches a specified value under the applied pressure for a given soil.

VALIDATION OF THE PROPOSED STERN MODEL

The proposed compressible Stern model was validated on five different bentonites from the literature and the validation results were presented in Fig. 8. A flowchart for the computation of the pressure-void ratio relationship based on the proposed approach was presented in Fig. 7. The

predicted compressibility data of these bentonites from the Gouy-Chapman model and the Stern model for CSP conditions (Tripathy et al., 2014) were also presented along with the proposed model to carry out a comparative analysis.

Table 2 presents the relevant properties of the bentonites used in the prediction of the compressibility data of the bentonites using the three models. The valence was taken as 1 for Na-dominated bentonites and 2 for Ca or other divalent cations–dominated bentonites in the Stern interacting CSP model as considered by Tripathy et al. (2014), while weighted average valence (ν_{avg}) was considered in the prediction by the Gouy-Chapman and the proposed model. The initial Stern layer thickness (δ_0) at zero pressure was considered to be equivalent to the hydrated radius Na^+ cation for the Na-dominated Na-Ca-MX80 bentonite and Mexico montmorillonite in the proposed model. For the other bentonites, which have either mixed-valence or divalent-dominated surface cations, the hydrated radius of Ca^{2+} cation was taken as the Stern layer thickness, being the largest among the available exchangeable cations. The Stern layer compression was applied when the potential ratio (u/y_δ) reached a specified value (R_y) for the given bentonite. However, a fixed value of 5 Å was used as the Stern thickness for all the bentonites in the CSP model by Tripathy et al. (2014). The pore fluid parameters and other relevant parameters used in the three models were presented in Table 3.

The predicted compressibility data by the proposed model and the two existing models were compared with the measured data for five different bentonites as presented in Fig. 8. The CSP model by Tripathy et al. (2014) was not in good agreement with the measured data in the studied pressure range for the studied bentonites. The CSP model was in close agreement with the measured data for the Na-Kunigel bentonite briefly in the lower pressure range of 0.1 – 0.5 MPa, however, deviated significantly at higher pressures (Fig. 8b). For the other studied bentonites, the

CSP model was far away from the measured data as compared to the proposed model (Fig. 8a, 8c-8e). The observed discrepancies were attributed to the issue with the assumption of constant surface potential conditions in the model, as discussed earlier. Overall, the Gouy-Chapman model was relatively close to the measured data as compared to the CSP model, however, severely underestimated the void ratios at large pressures. This was primarily due to not considering the effect of the size of the cation in the Gouy-Chapman theory. The proposed model based on the Stern theory at CSC condition showed a better agreement with the measured data in the studied pressure range in comparison to the existing two models. The proposed model significantly improved the prediction at large pressures as the predicted void ratios were higher than the Gouy-Chapman model due to the incorporation of the size of the cations and were very close to the measured data. Further, treatment of the compressible Stern layer provided a realistic void ratio variation with pressure at very large pressures unlike the earlier Stern model at CSP condition. Overall, the proposed model showed a better prediction at pressures higher than 0.1 MPa for the studied bentonites, however, overpredicted at a lower pressure range (0.01 MPa- 0.1 MPa). The observed discrepancies at lower pressures were attributed to the dominant presence of the edge-face clay platelets orientation as the theory is based on the parallel arrangement of the clay platelets.

CONCLUSIONS

The effect of cations size was incorporated into the prediction of clay compressibility behavior using the Stern theory at CSC condition for the first time. A mathematical model was developed to establish the potential-distance relationship for the interacting Stern model at the CSC condition. The compressibility of the Stern layer was further incorporated into the theory for the first time to provide a more realistic prediction of the compressibility behavior of bentonites in the high-

pressure range. Based on the detailed analysis of the compressibility data of different bentonites from the literature using the proposed Stern theory, the following conclusion was drawn.

Under the application of load, the diffused Gouy layer initially undergoes significant compression, while the Stern layer remains unaffected. The compression of the Stern layer starts in the pressure range of 0.5–1 MPa for different bentonites once the thickness of the Gouy layer is significantly reduced. The thickness of the Stern layer reaches a minimum value equivalent to the water molecule size at a pressure of ~40 MPa. The siloxane cavities on the surface of the clay platelets accommodate the cations at such high pressure to facilitate the Stern layer compression. The void ratio corresponding to the minimum Stern layer thickness at such high pressure is ~0.4.

The ratio of the midplane to Stern potential, which represents the degree of interaction in the clay-water system, influenced the compression behavior of the Stern layer under the loading. The potential ratio of the clay-water electrolyte system at any given pressure is dependent on the type and composition of the exchangeable cations on the clay surface. The Stern layer compression starts when the potential ratio is in the range of 0.65-0.75 for bentonites with different surface cations characteristics.

DECLARATION

Funding: This research received no specific grant from any funding agency in the public, commercial, or not-for-profit sectors.

Conflicts of interest: All the authors declare that they have no conflicts of interest.

Availability of data: The datasets generated during and/or analyzed during the current study are available from the corresponding author on reasonable request.

Code availability: The codes developed and/or used in the current study are available from the corresponding author on reasonable request.

Appendix

The estimation of Stern layer charge (σ_1) in an interacting system for CSC conditions is not available due to the difficulties involved in estimating the two parameters, such as the number of available adsorption sites and specific adsorption potential on the counter-ions at the clay surface (see Eq. 9). The influence of platelet interaction on the number of available adsorption sites is not understood yet. Further, the specific adsorption potential, ψ for a given clay-water-electrolyte system is difficult to estimate under varying DDL interaction. The σ_1 estimation was, therefore, eliminated by considering

$$\frac{\sigma}{\sigma_2} = \frac{A_{Stern}}{A_{Gouy}} + 1 \tag{A1}$$

Substituting the expression for the Gouy layer charge (σ_2) from Eq. (10) in Eq. (A1) and re-arranging gives

$$\sigma A_{Gouy} = \sqrt{2nkT\varepsilon}\sqrt{2\cosh y_\delta - 2\cosh u}\left(A_{Stern} + A_{Gouy}\right) \tag{A2}$$

The area of Stern layer was estimated from Eq. (A3).

$$A_{Stern} = \frac{\left(y_0 + y_\delta\right)}{2}\delta \tag{A3}$$

After substituting for y_0, from Eq. (6),

$$A_{Stern} = \left(y_\delta + \left(vq\sigma 2\pi\delta/\varepsilon' kT\right)\right)\delta \tag{A4}$$

Combining Eqs. (A1) and (A3), we get

$$\sigma A_{Gouy} = \sqrt{2nkT\varepsilon}\sqrt{2\cosh y_\delta - 2\cosh u}\left(\left(y_\delta + \left(vq\sigma 2\pi\delta/\varepsilon' kT\right)\right)\delta + A_{Gouy}\right) \quad \text{(A5)}$$

The area under the hyperbolic potential distribution curve for the Gouy layer (A_{Gouy}) can be calculated by following the method of slices. Dividing the entire Gouy layer thickness into *N* number of thin slices of equal thickness Δx , the area can be computed as,

$$A_{Gouy} = \sum_{i=1}^{N+1} \frac{\left(y_i + y_{i+1}\right)}{2}\Delta x \quad \text{(A6)}$$

where $y_{i+1} = y_i - (slope)_i \Delta x$, and *i* denotes the number of nodal points, $d = N\Delta x$. The boundary conditions are– $y_i = y_\delta$ at *i=1*, and $y_i = u$ at *i* = N+1. The slope of the potential distribution in the Gouy layer at any point can be obtained as per the following equation,

$$\left(slope\right)_i = \kappa\sqrt{2\cosh y_i - 2\cosh u} \quad \text{(A7)}$$

The Gouy area, thus, can be estimated by knowing the Stern and mid-plan potentials in an interacting clay-water-electrolyte system.

REFERENCES

Baille, W., Tripathy, S., & Schanz, T. (2010) Swelling pressures and one-dimensional compressibility behavior of bentonite at large pressures, *Applied Clay Science*, *48(3),* 324-333.

Benson, C. H., Zhai, H., Wang, X. (1994) Estimating hydraulic conductivity of compacted clay liners. J. Geotech. Eng. 120, 366-387.

Bharat, T.V. & Sridharan, A. (2015a) Prediction of compressibility data for highly plastic clays using diffuse double-layer theory, *Clays and Clay Minerals*, *63*, 30-42.

490 Bharat, T.V. & Sridharan, A. (2015b) A critical appraisal of debye length in clay-electrolyte
491 systems, *Clays and Clay Minerals*, *63*, 43-50.

492 Bharat, T.V., Sivapullaiah, P.V., & Allam, M.M. (2009) Swarm intelligence-based solver for
493 parameter estimation of laboratory through-diffusion transport of contaminants, *Computers and*
494 *Geotechnics*, *36*, 984-992

495 Bharat, T.V., Sivapullaiah, P.V., & Allam, M.M. (2013) Novel procedure for the estimation of
496 swelling pressures of compacted bentonites based on diffuse double layer theory, *Environmental*
497 *Earth Science*, *70*, 303-314.

498 Bishop, A. W. (1959) The principle of effective stress. Teknisk Ukeblad, 39, 1859-863.

499 Bolt, G. H. (1956) Physico-chemical analysis of compressibility of pure clays. *Geotechnique*, 46,
500 291–311.

501 Bucher, F., & Müller-Vonmoos, M. (1989) Bentonite as a containment barrier for the disposal of
502 highly radioactive wastes. *Appl. Clay Sci.*, 4(2), 157-177.

503 Burland, J. B. (1990) On the compressibility and shear strength of natural clays, *Geotechnique*,
504 *40*, 329–378.

505 Chapman, D. L. (1913) A contribution to the theory of electrocapillarity, *The London, Edinburgh,*
506 *and Dublin philosophical magazine and journal of science*, *25(148),* 475-481.

507 Chen, Y. G., Zhu, C. M., Ye, W. M., Cui, Y. J., Chen, B. (2016) Effects of solution concentration
508 and vertical stress on the swelling behavior of compacted GMZ01 bentonite. *Appl. Clay Sci.* 124,
509 11-20.

510 Das, D., & Tadikonda, V. B. (2021) Specific Surface Area of Plastic Clays from Equilibrium
511 Sediment Volume under Salt Environment, *Geotechnical Testing Journal*, *44(5),* 1484-1500.

512 Delage, P., & Lefebvre, G. (1984) Study of the structure of a sensitive Champlain clay and of its
513 evolution during consolidation, *Canadian Geotechnical Journal*, *21(1)*, 21-35.

514 Di Maio, C., Santoli, L., & Schiavone, P. (2004) Volume change behavior of clays: the influence
515 of mineral composition, pore fluid composition and stress state, *Mechanics of Materials, 36*, 435-

451.

ENRESA (2000) Full-scale engineered barriers experiment for a deep geological repository for high-level radioactive waste in crystalline host rock (FEBEX project) EUR, 19147 (2000) (Nuclear Science and Technology Series. Luxembourg. 362 pp.)

Glatstein, D. A., Francisca, F. M. (2015) Influence of pH and ionic strength on Cd, Cu and Pb removal from water by adsorption in Na-bentonite. *Appl. Clay Sci*., 118, 61-67.

Gouy, G. (1910) Electrical charge on the surface of an electrolyte, *Journal of Physics*, *4*, 457–468

Grim, R. E. (1968) *Clay mineralogy*, 2nd edn. McGraw-Hill, New York

Guven, N., & Pollastro, R.M. (Editors). (1992) Clay-water interface and its rheological implications, CMS workshop lectures, vol. 4, The Clay Minerals Society, Boulder, Colo.

Honig, E. P., & Mul, P. M. (1971) Tables and equations of the diffuse double layer repulsion at constant potential and at constant charge. *J. Colloid and Interface Sci.*, 36(2), 258-272.

Hunter, R. J. (1981) *Zeta potential in colloid science,* Academic press Inc., London

Ishikawa, H., Amemiya, K., Yusa, Y., & Sasaki, N. (1990) Comparison of fundamental properties of Japanese bentonites as buffer material for waste disposal. *Sciences Géologiques, bulletins et mémoires*, 87(1), 107-115.

Israelachvili, J. N. (2011) *Intermolecular and surface forces*. Academic press.

Japan Nuclear Cycle Development Institute. (1999) H12: Project to Establish the Scientific and Technical Basis for HLW Disposal in Japan, Supporting Report 2, Repository Design and Engineering Technology

Jiang, X., Zhou, J., Zhu, M., He, W., & Yu, G. (2001) Charge characteristics on the clay surface with interacting electric double layers, *Soil science, 166(4),* 249-254.

Kaufhold, S., Baille, W., Schanz, T., & Dohrmann, R. (2015) About differences of swelling pressure—dry density relations of compacted bentonites. *Appl. Clay Sci.,* 107, 52-61.

Komine, H., & Ogata, N. (2003) New equations for swelling characteristics of bentonite-based buffer materials. *Canadian Geotechnical Journal,* 40(2), 460-475.

Lambe, T. W. (1960) Discussion on factors controlling the strength of partly saturated cohesive soils. *Conf. Shear Strength Soils. Colorado*, 1094-1095.

Lambe, T. W. and Whitman, R. V. (2008) *Soil mechanics SI version.* John Wiley & Sons.

Langmuir, I. (1938) The role of attractive and repulsive forces in the formation of tactoids, thixotropic gels, protein crystals, and coacervates, *The Journal of Chemical Physics, 6(12),* 873-896.

Low, P.F. (1980) The swelling of clay: II. Montmorillonites, *Soil Science Society of America Journal, 4,* 667–676.

Lu, N., & Likos, W. J. (2006) Suction stress characteristic curve for unsaturated soil. *J. Geotech. Geoenviron. Engg.,* 132(2), 131-142.

Marcial D., Delage P., & Cui Y.J. (2002) On the high-stress compression of bentonites, *Can. Geotech. J., 39,* 812–820

Mitchell, J. E. (1960) *The application of colloidal theory to the compressibility of clays. Interparticle forces in clay-water-electrolyte systems*, Melbourne: CSIRO, 2.92-2.98.

Mitchell, J. K., & Soga, K. (2005) *Fundamentals of soil behavior*, New York: John Wiley & Sons.

Nagaraj, T. S., & Murthy, S. B. R. (1986) A critical reappraisal of compression index equations, *Geotechnique, 36*, 27-32.

Olsen RE, Mesri G. (1970) Mechanisms controlling compressibility of clays. *J Soil Mech & Found Div ASCE*: 96, No. SM 6:1863–1878.

Peirce, J. J., Sallfors, G., & Murray, L. (1986) Overburden pressures exerted on clay liners, *Journal of Environmental Engineering, 112*, 280-291.

Pusch, R. (2015) *Bentonite Clay: Environmental Properties and Applications*. Taylor & Francis,

Pusch, R., Yong, R., & Nakano, M. (2011) *High-level radioactive waste (HLW) disposal: A global challenge.* WIT Press.

Schubert, H. (1975) Tensile strength of agglomerates. *Powder Technology*, 11(2), 107-119.

567 Shang, J. Q., Lo, K. Y., & Quigley, R. M. (1994) Quantitative determination of potential
568 distribution in Stern-Gouy double-layer model, *Canadian Geotechnical Journal, 31(5)*, 624–636.

569 Skempton, A. W. (1960) The pore-pressure coefficient in saturated soils. *Géotechnique,* 10(4),
570 186-187.

571 Sparks, D. L., (1999) *Soil Physical Chemistry*. 2nd edition, Boca Raton: CRC Press.

572 Sposito, G. (1984) *The surface chemistry of soils*, Oxford university press.

573 Sposito, G. (2008) *The chemistry of soils*, 2nd edn. Oxford University press, New York

574 Sridharan, A. & Venkatappa Rao, G. (1970) Basic mechanisms controlling volume changes in
575 clays. Publication 35, Annual Report of the Department of Civil and Hydraulic Engineering, Indian
576 Institute of Science, Bangalore, India.

577 Sridharan, A. & Venkatappa Rao, G. (1972) Physico-chemical mechanisms controlling the
578 strength, con- solidation and swelling behaviour of clays*, Symp. strength and deformation of soils*,
579 Bangalore, India.

580 Sridharan, A. (1968) Some studies on the strength of partly saturated clays, PhD thesis, Purdue
581 University, West Lafayette

582 Sridharan, A., & Choudhury, D. (2002) Swelling pressure of sodium montmorillonites.
583 *Géotechnique*, 52(6), 459-462.

584 Sridharan, A., & Jayadeva, M. S. (1982) Double layer theory and compressibility of clays.
585 *Geotechnique*, 32(2), 133-144.

586 Sridharan, A., & Rao, G. V. (1973) Mechanisms controlling volume change of saturated clays and
587 the role of the effective stress concept. *Geotechnique*, 23(3), 359-382.

588 Sridharan, A., & Satyamurty, P. V. (1996) Potential-distance relationships of clay-water systems
589 considering the stern theory, *Clays and Clay Minerals, 44(4),* 479–484.

590 Stern, O. (1924) Zur theorie der elektrolytischen doppelschicht, *Zeitschrift für Elektrochemie und*
591 *angewandte physikalische Chemie, 30(21- 22),* 508-516.

592 Timmons, J., Cho, Y. M., Townsend, T., Berge, N., & Reinhart, D. (2012) Total earth pressure
593 cells for measuring loads in a municipal solid waste landfill, *Geotechnical & Geological*
594 *Engineering, 30*, 95-105.

595 Tripathy, S. and Schanz, T. (2007) Compressibility behaviour of clays at large pressures. *Can.*
596 *Geotech. J.*, 44, 355–362.

597 Tripathy, S., Bag, R., & Thomas, H. R. (2014) Effect of Stern-layer on the compressibility behavior
598 of bentonites, *Acta Geotechnica, 9(6),* 1097–1109.

599 Tripathy, S., Sridharan, A., Schanz, T. (2004) Swelling pressures of compacted bentonites from
600 diffuse double layer theory. *Can. Geotech. J.,* 41, 437-450.

601 van Olphen, H. (1964) Internal mutual flocculation in clay suspensions, *Journal of Colloid*
602 *Science, 19(4),* 313–322.

603 van Olphen, H. (1977) *An introduction to clay colloid chemistry: for clay technologists, geologists*
604 *and soil scientists*, 2nd edn. Interscience, New York

605 Verwey, E. J. W., & Overbeek, J. T. G. (1955) Theory of the stability of lyophobic colloids,
606 *Journal of Colloid Science*, *10(2),* 224–225.

607 Verwey, E. J. W., Overbeek, J. T. G., & Van Nes, K. (1948) *Theory of the stability of lyophobic*
608 *colloids: the interaction of sol particles having an electric double layer,* Elsevier Publishing
609 Company.

610 Ye, W. M., Zhang, F., Chen, B., Chen, Y. G., Wang, Q., & Cui, Y. J. (2014) Effects of salt solutions
611 on the hydro-mechanical behavior of compacted GMZ01 bentonite, *Environmental Earth Science,*
612 *72,* 2621-2630.

613 Zheng, L., Rutqvist, J., Xu, H., & Birkholzer, J. T. (2017) Coupled THMC models for bentonite
614 in an argillite repository for nuclear waste: Illitization and its effect on swelling stress under high
615 temperature. *Engineering geology*, 230, 118-129.

616

617

618

619 Table 1. Parameters used to establish electrostatic potential distribution in the Gouy-Chapman
620 model and the proposed Stern model (Fig. 3 & 4)

Parameters	Value
Specific gravity, G_s	2.76
Specific surface area, S_a (m^2/g)	800
Cation Exchange Capacity, C_e (meq/100g	100
Valence, ν	1
Dielectric constant of bulk pore fluid, ε	80.4
Stern thickness/hydrated cationic radius, δ (Å)	7.9
Dielectric constant of water within stern layer, ε'	6
Temperature, T (K)	298

621

622 Table 2. Relevant bentonite properties used in the theoretical prediction of compressibility
623 behavior

Soil name	S_a (m^2/g)	Total C_e (meq/100g)	Individual cations				v_{avg}	G	δ_0 (Å)
			Na^+	Ca^{2+}	Mg^{2+}	K^+			
MX80 bentonite[a]	676	90.31	51.24	28.24	9.43	1.28	1.42	2.76	9.6
Na-Ca MX80 bentonite[b]	700	68	60	5	3	-	1.12	2.65	7.9
Na-Kunigel[b]	687	73.2	40.5	28.7	3	0.9	1.45	2.79	9.6
Ponza[c]	500	85	14	22	46	-	1.76	2.77	9.6
Mexico Montmorillonite[d]	734	114	92	1	-	1	1	2.7	7.9

624 [a]Tripathy et al. (2014), [b]Marcial et al. (2002), [c]Di Maio (2002), [d]Low (1980),

625 Table 3. Parameters used in the prediction of compressibility behavior of the considered bentonites
626 by the three models

Parameters	Value		
	GC	Stern constant potential	proposed
Cationic concentration, n (N)	0.0001	0.0001	0.0001
Valence, ν	$^{*}\nu_{avg}$	$^{\#}$1 or 2	$^{*}\nu_{avg}$
Dielectric constant of water	80.4	80.4	80.4
Stern thickness, δ(Å)	N/A	5	$^{\$}\delta_0$
Dielectric constant of Stern pore fluid, ε'	N/A	6	6
Surface potential, ϕ_0(mV)	N/A	274	N/A
Normalized surface potential, y_0	N/A	10.66	N/A
Specific adsorption potential, ψ	N/A	0	N/A
Number of adsorption spot, N_1 (ions/m^2)	N/A	$^{\&}4.10^{-17}$	N/A
Density of water, ρ_w (Mg/m^3)	1	1	1
Molecular weight of solvent (water), M (Mg/mol)	N/A	18	N/A
T (K)	298	298	298

627 *weighted average valence (see Table 2), $^{\#}$1 for Na-d0minated and 2 for di-valence dominated,
628 $^{\$}$initial Stern layer thickness at zero pressure (see table 2), $^{\&}$for Na^+.

629

630 **Table 4. List of figures**

Figure	Caption
Fig. 1	Illustration showing interaction of DDL of two approaching clay platelets under applied mechanical pressure
Fig. 2	Electric potential distribution in Stern DDL model
Fig. 3a	Nature of objective function at 0.0001 M pore fluid concentration for three different pressure values

Fig. 3b	Nature of objective function at 10 kPa pressure for four different pore fluid concentrations
Fig. 4a	Computed electrostatic potential distribution in clay-water system (n = 0.0001M) based on GC and stern model under two different applied mechanical pressure
Fig. 4b	Variation of Stern potential and midplane potential in clay-water system (n = 0.0001M) with change in the degree of interaction (separation distance) under loading
Fig. 5a	Variation of DDL thickness with applied mechanical pressure derived from the measured compressibility data (using Eq. 4 with the parallel plate assumption) of different quality bentonites
Fig. 5b	Illustration showing cations penetrating the siloxane cavities on clay surface resulting in compression of Stern layer under very high applied mechanical pressure
Fig. 6a	Variation of double layer thickness with pressure at different degree of interaction for Ponza bentonite
Fig. 6b	Variation of double layer thickness with pressure at different degree of interaction for Na-Kunigel Bentonite
Fig. 6c	Variation of double layer thickness with pressure at different degree of interaction for Na-Ca-MX80 bentonite
Fig. 7	Flow chart showing the computation of void ratio at a given pressure using the proposed Stern model
Fig. 8a	Theoretically predicted and measured pressure-void ratio data of Na-Ca MX80 bentonite (Marcial et al., 2002)
Fig. 8b	Theoretically predicted and measured pressure-void ratio data of Na-Kunigel bentonite (Marcial et al., 2002)
Fig. 8c	Theoretically predicted and measured pressure-void ratio data of MX-80 bentonite (Tripathy et al., 2014)
Fig. 8d	Theoretically predicted and measured pressure-void ratio data of Ponza bentonite (Di Maio, 2011)
Fig. 8e	Theoretically predicted and measured pressure-void ratio data of Mexico Montmorillonite (Low 1980)

631

Pasted Layer

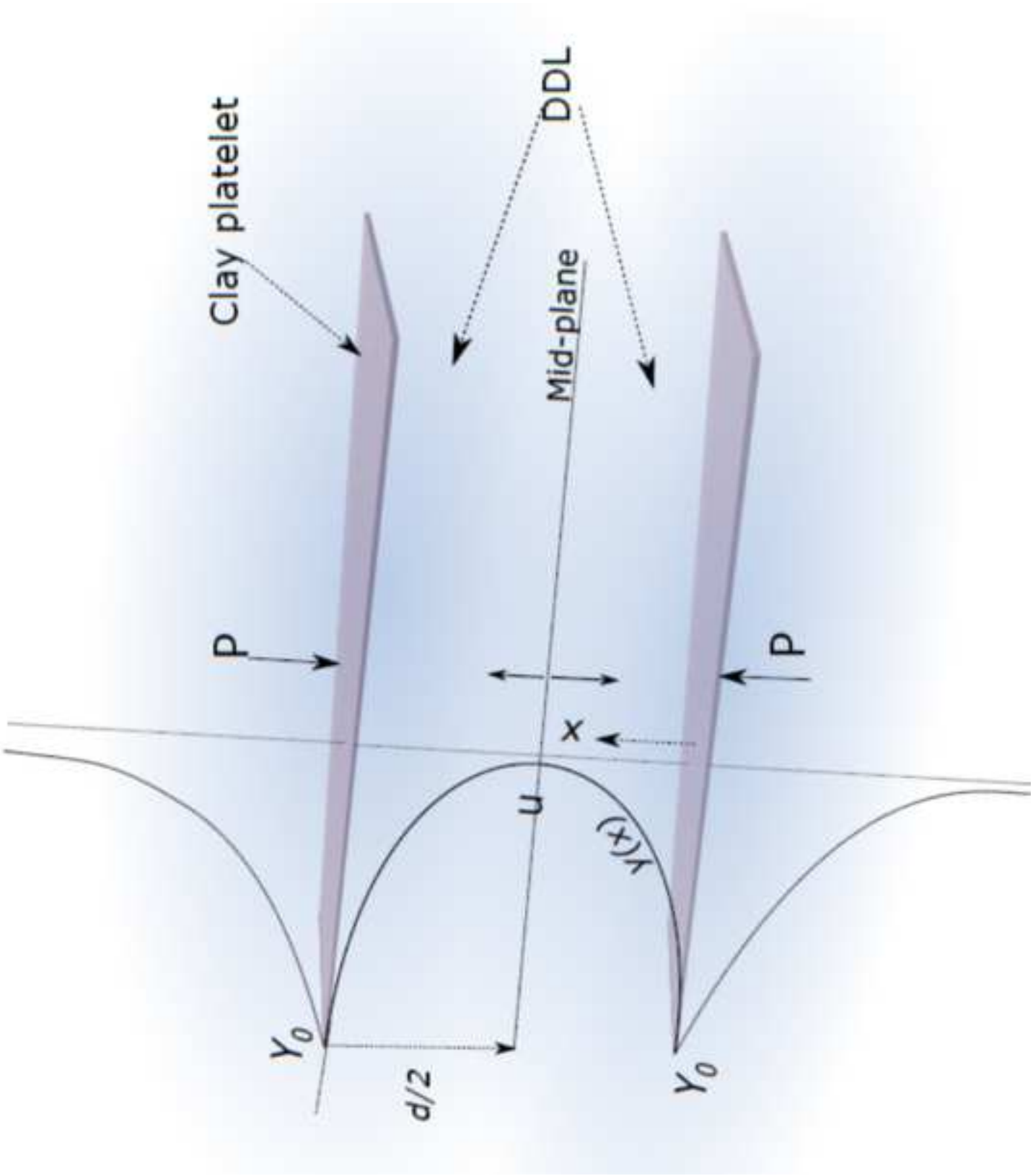

Fig.1

Pasted Layer

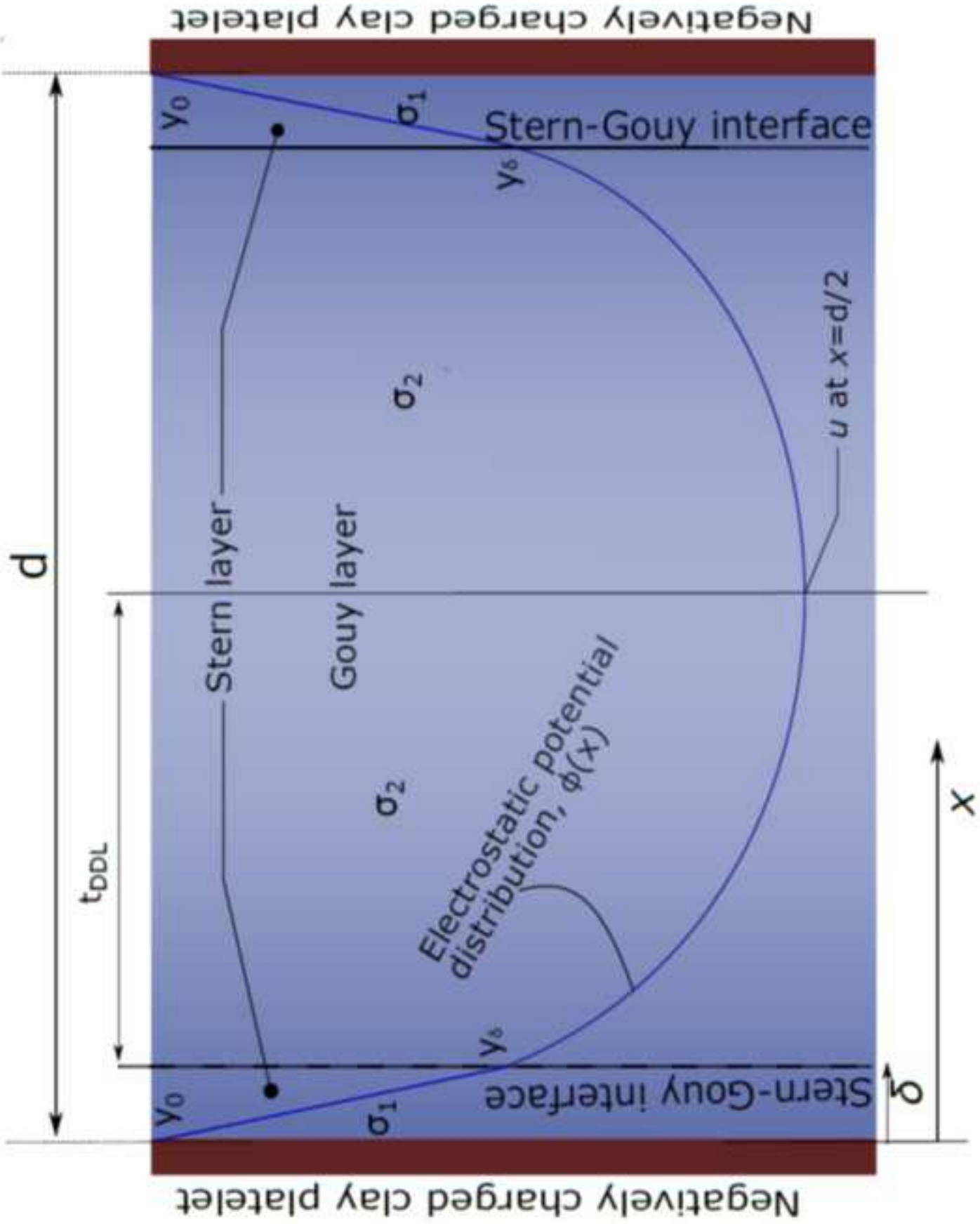

Fig.2

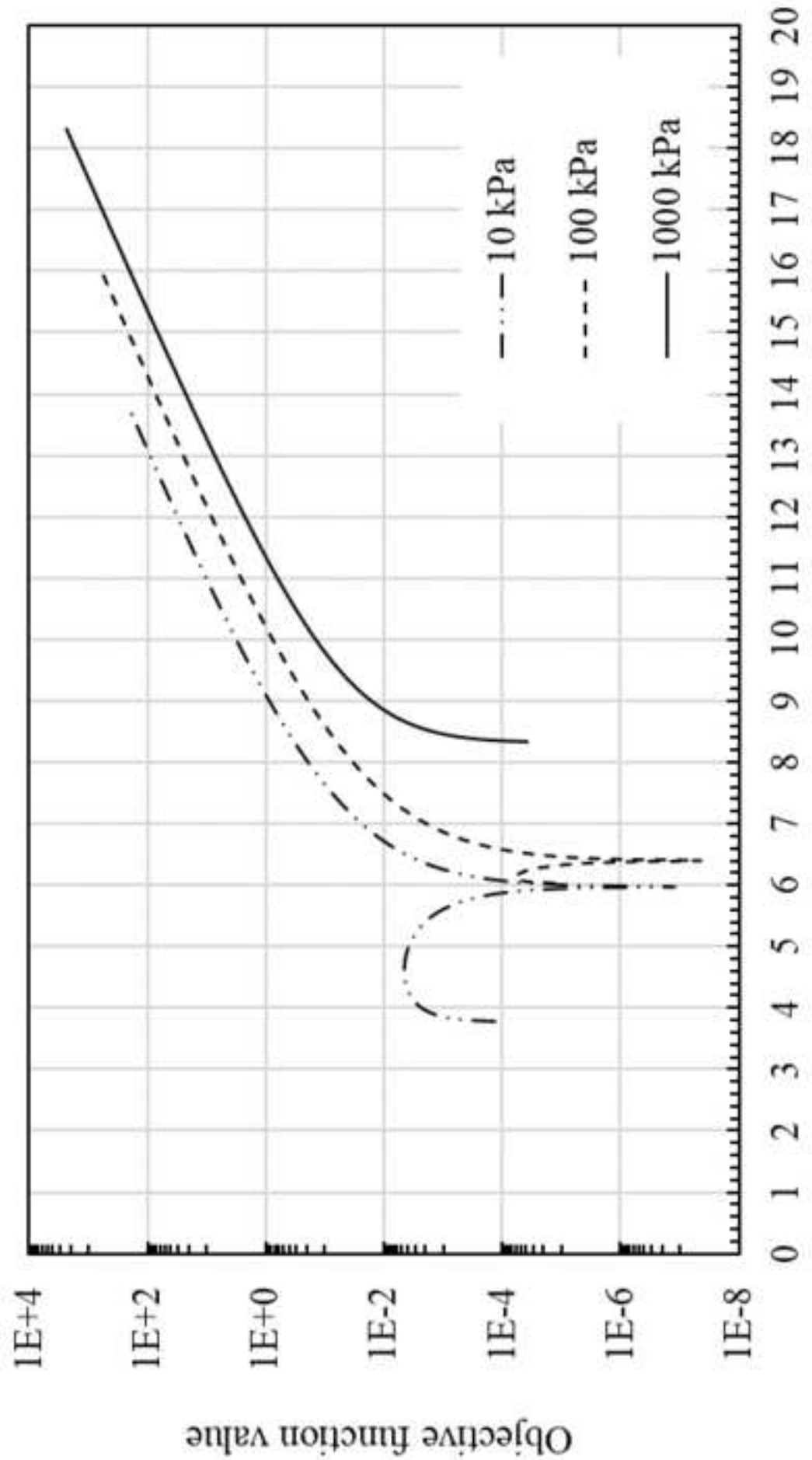

Fig.3a

Pasted Layer

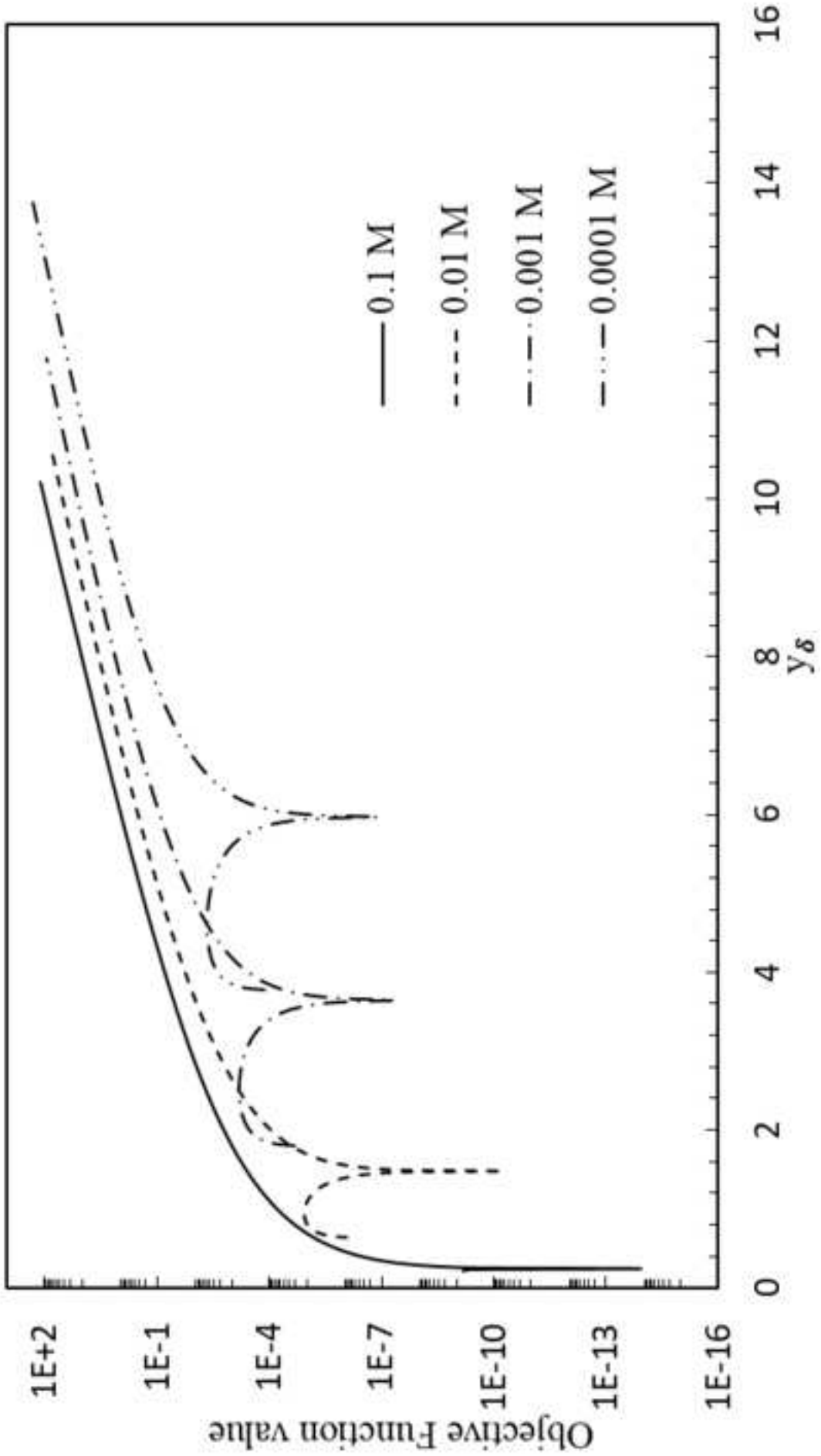

Fig.3b

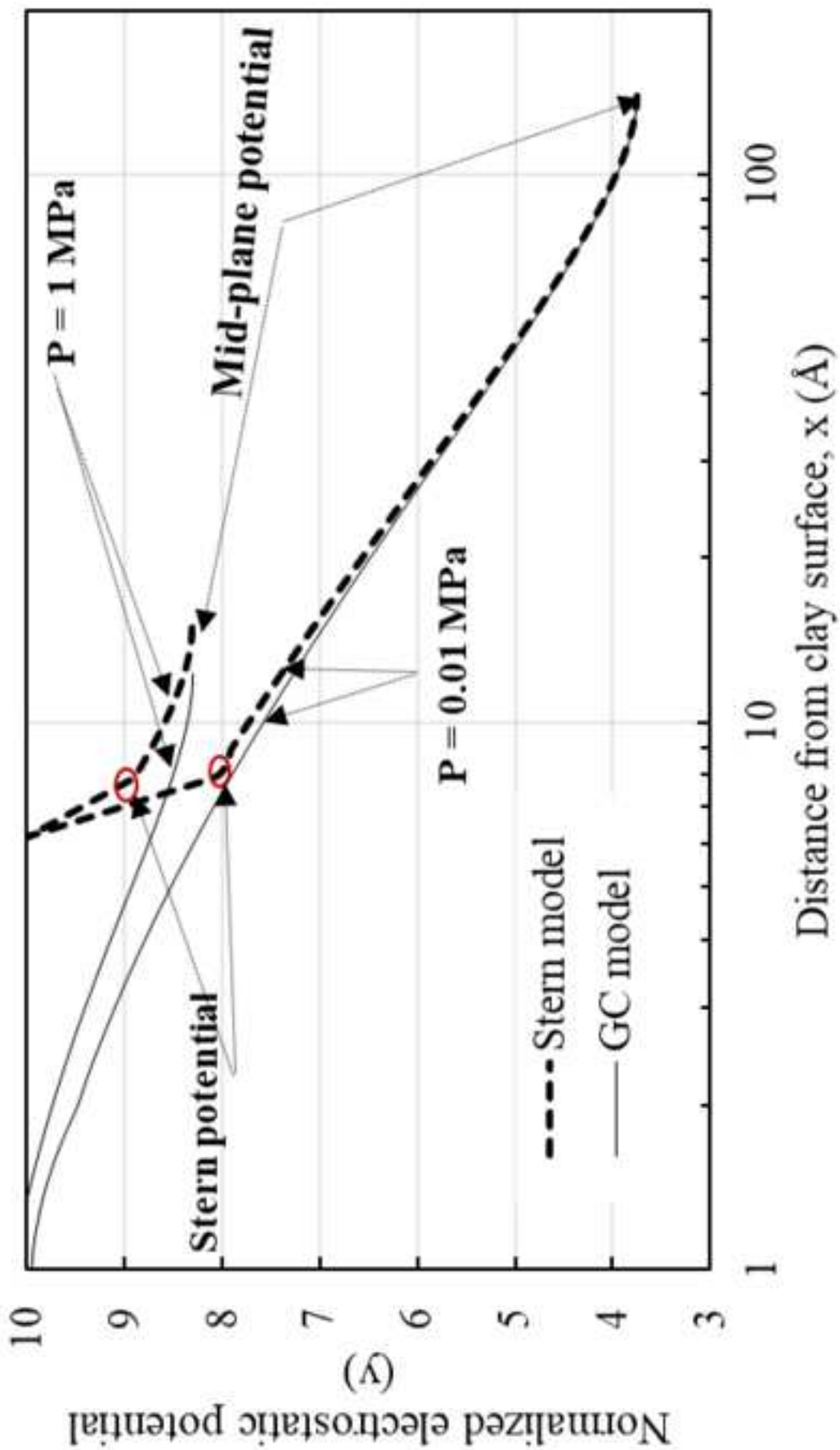

Fig.4a

Pasted Layer

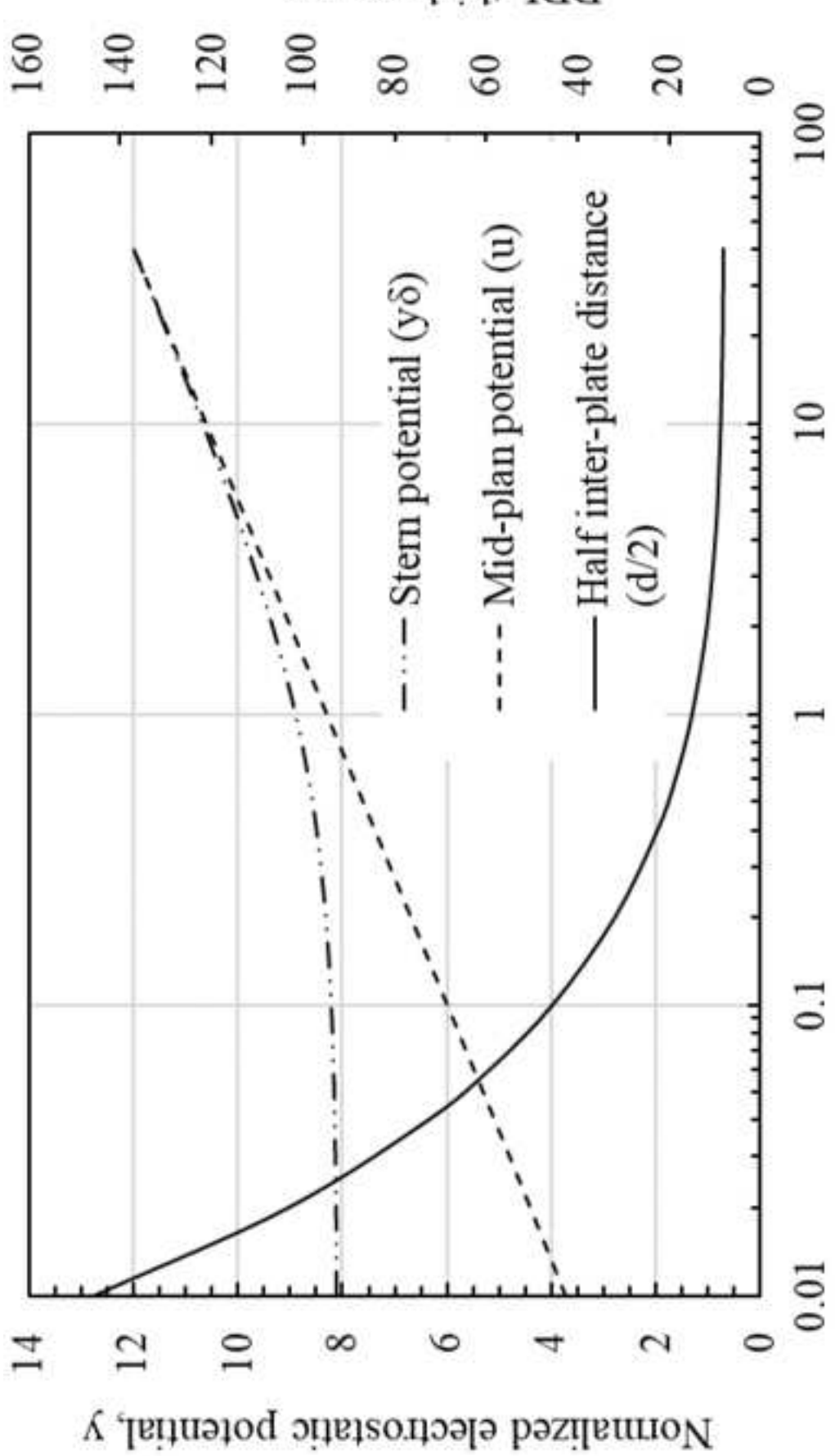

Fig.4b

Pasted Layer

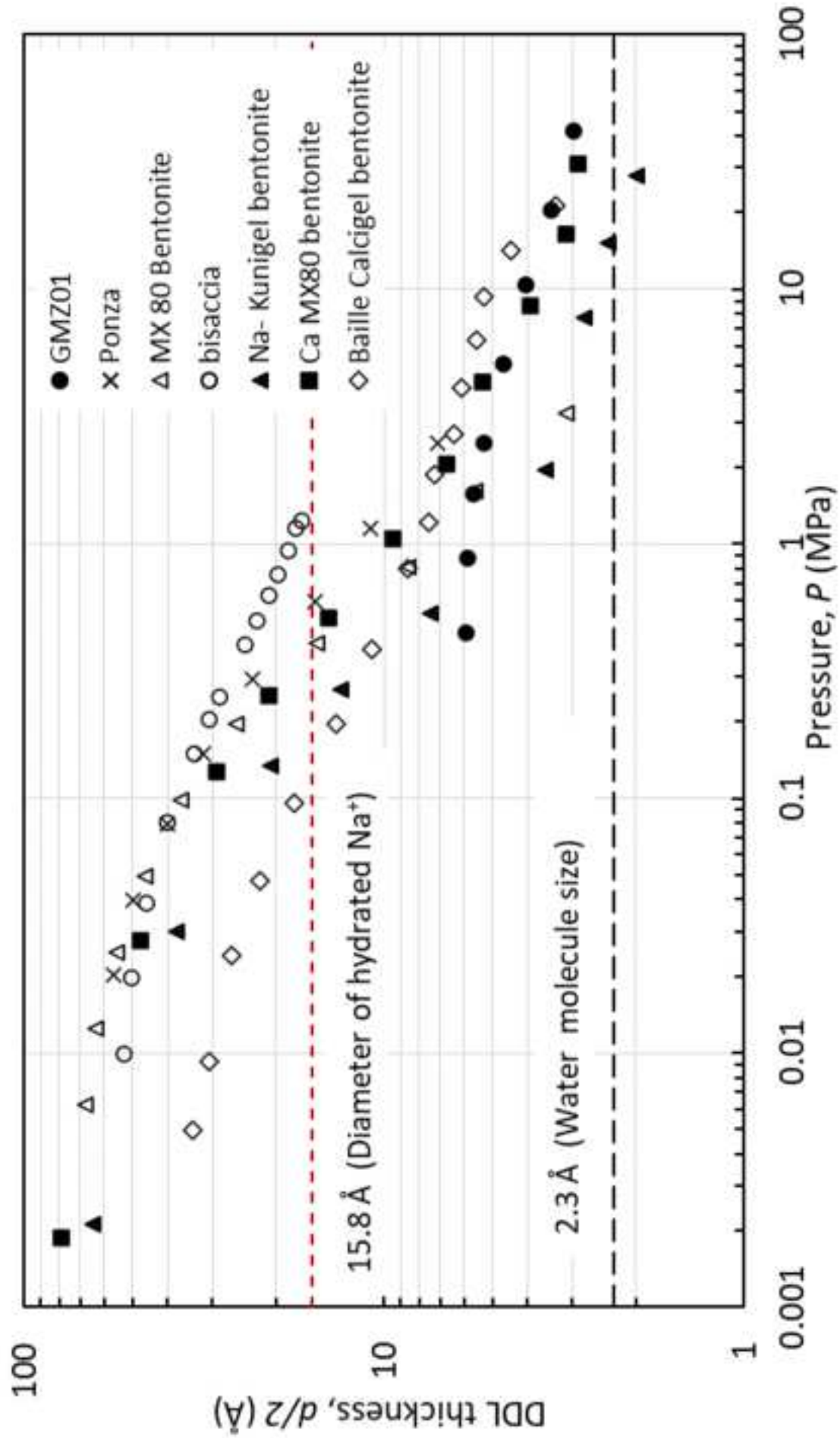

Fig.5a

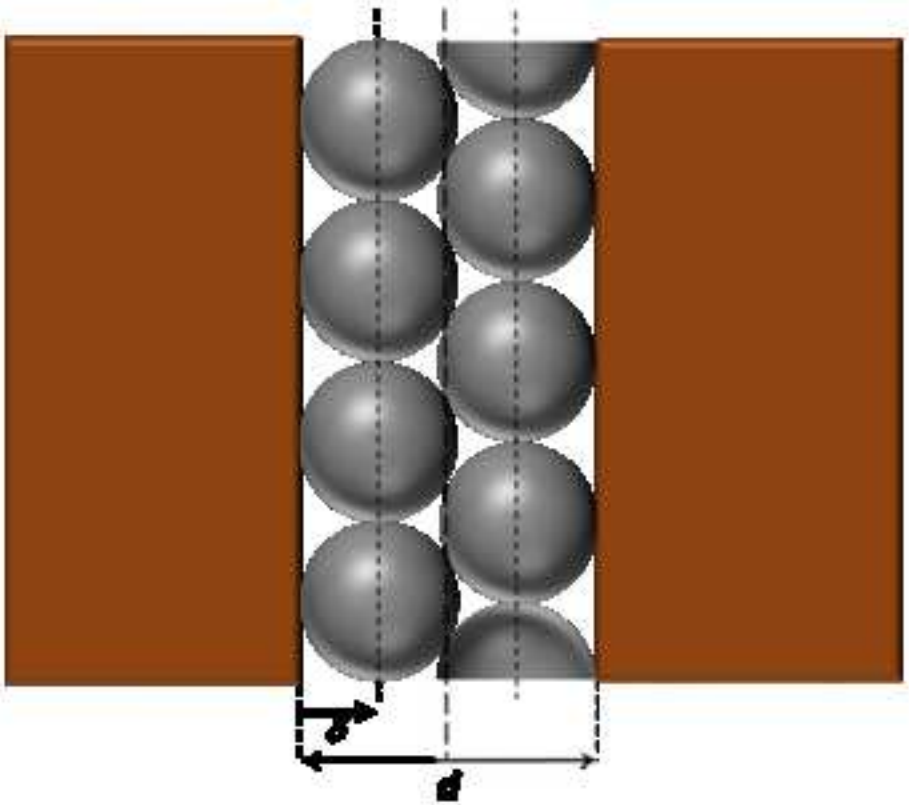

(i) Separation distance beyond which stern layer starts compressing

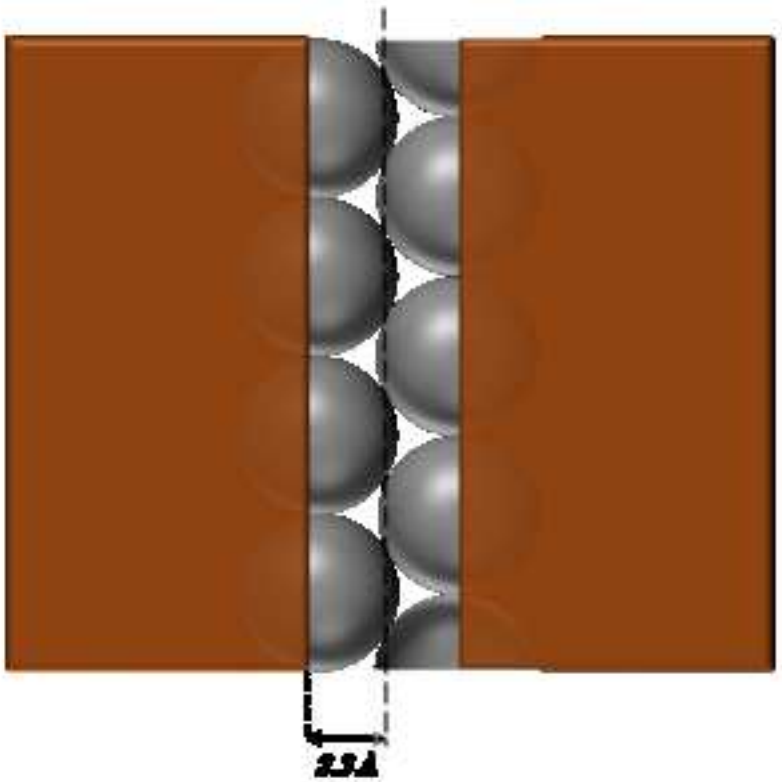

(ii) Minimum separation distance after penetration of the cations into the siloxane cavities

Pasted Layer

Pasted Layer

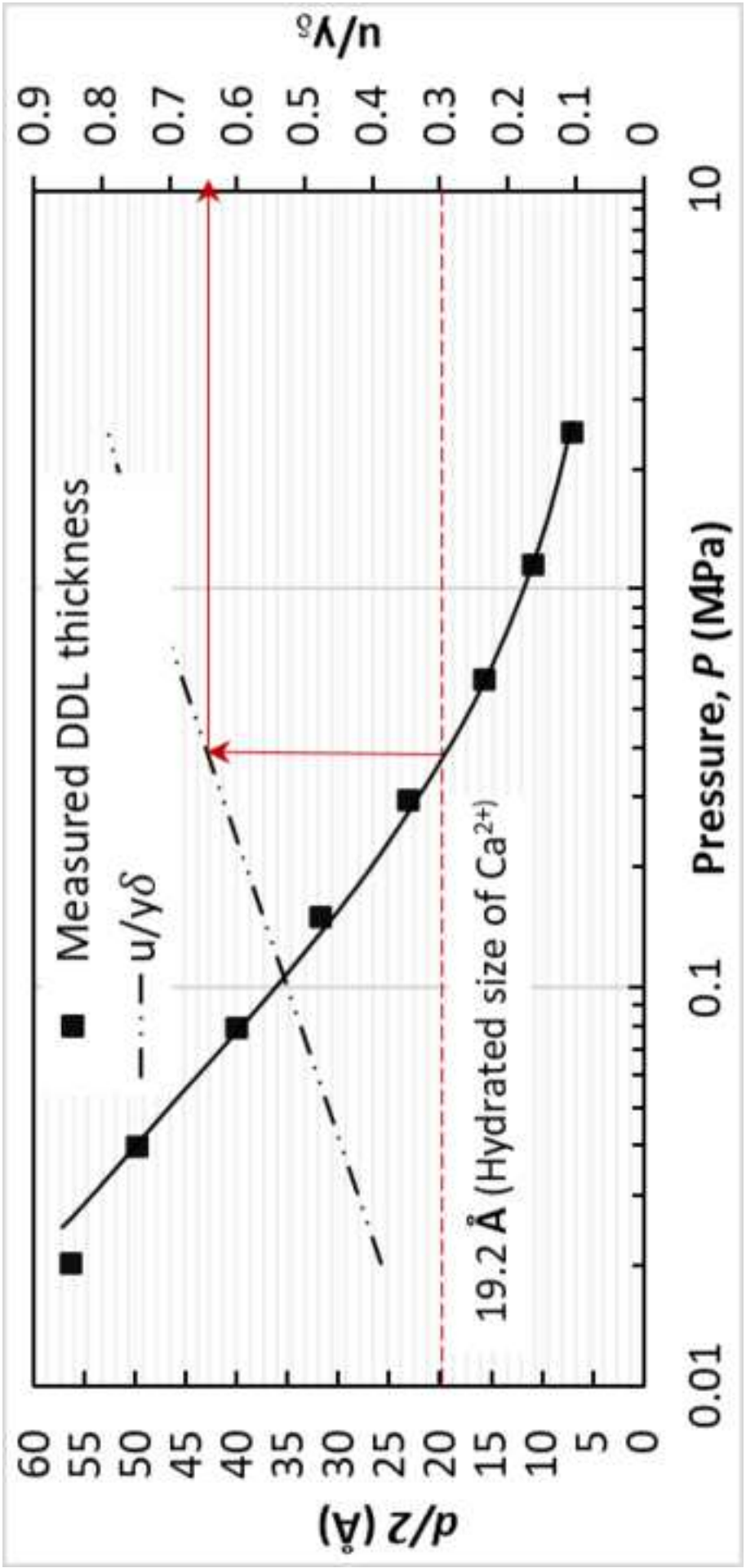

Fig.6a

Pasted Layer

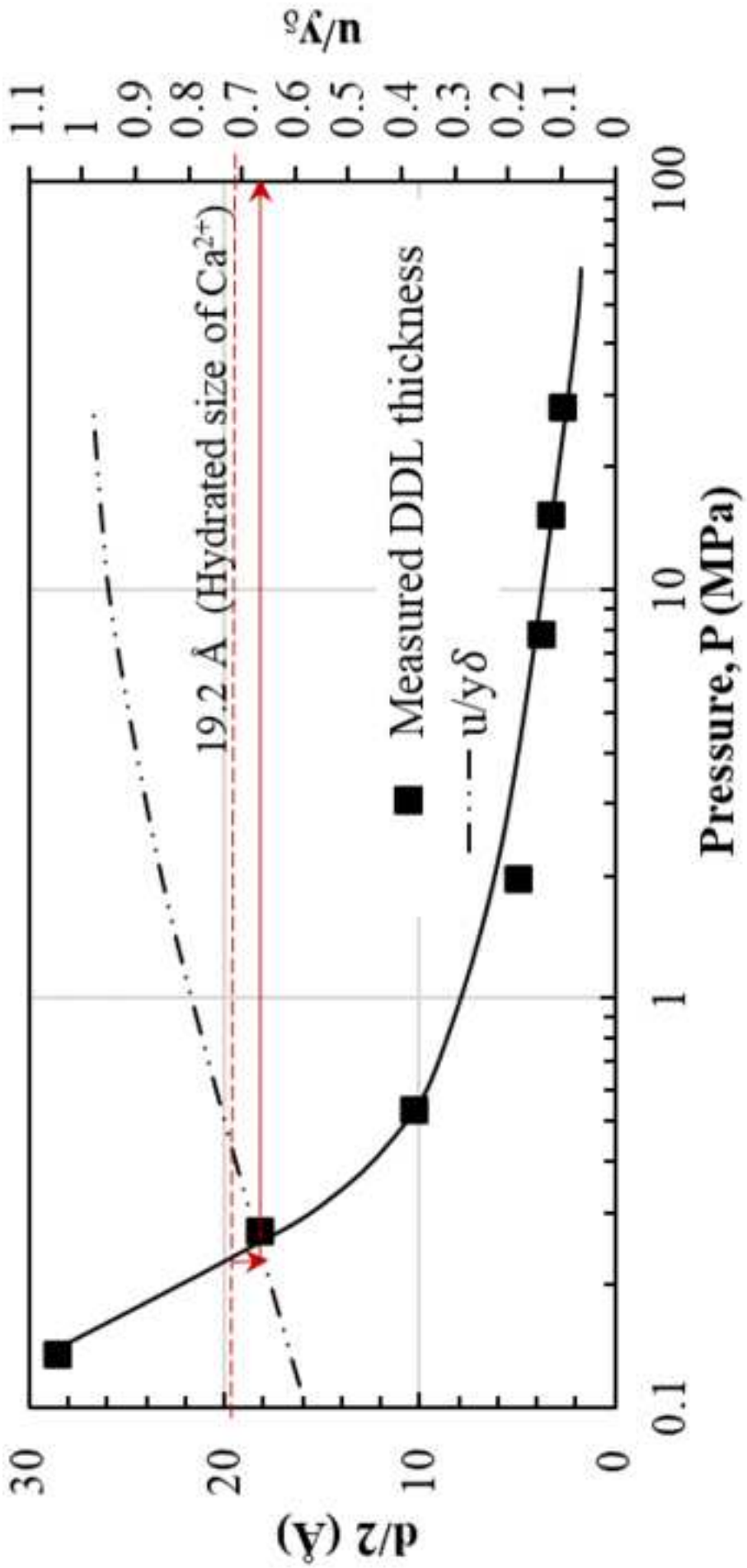

Fig.6b

Pasted Layer

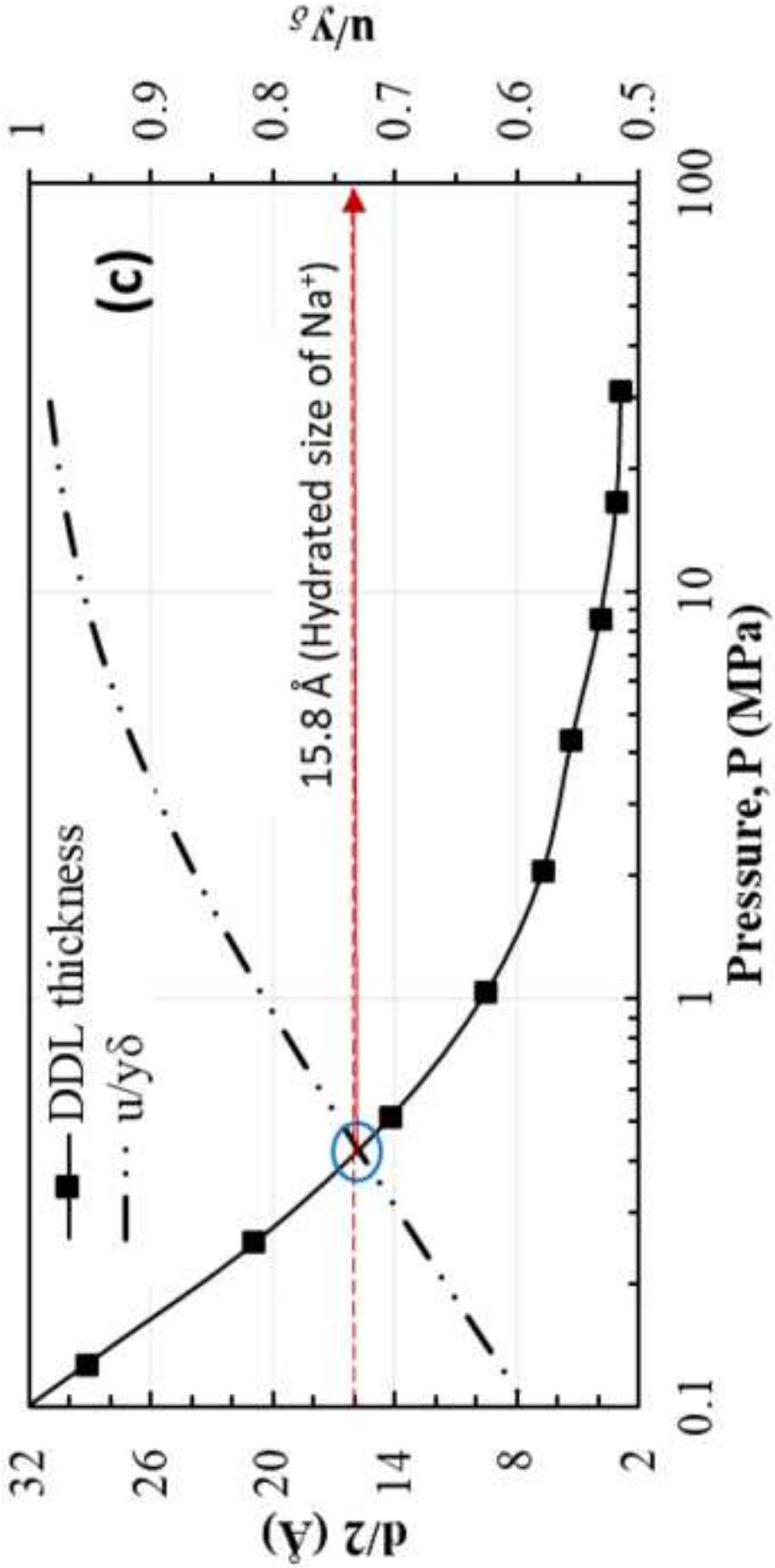

Fig.6c

Pasted Layer

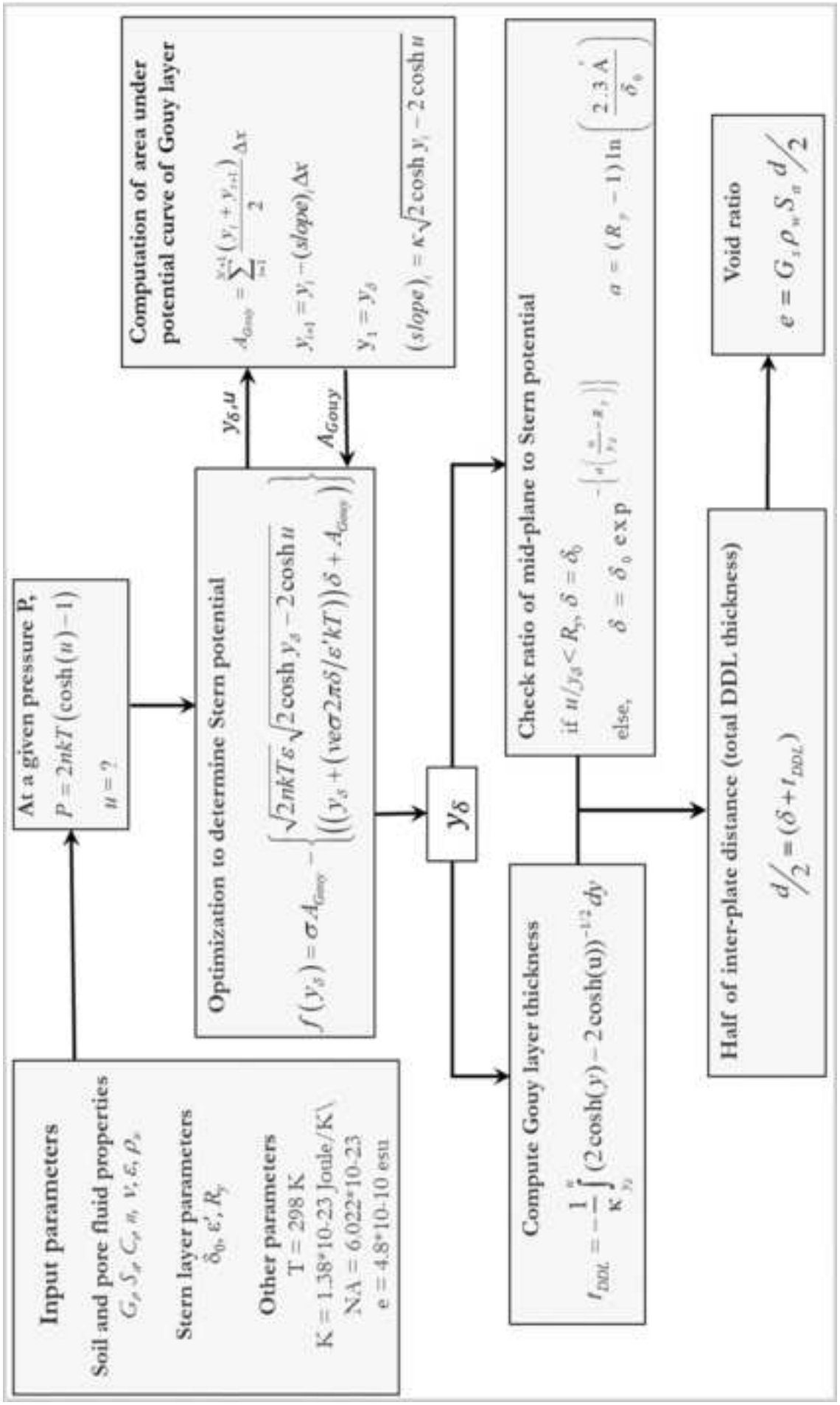

Fig.7

Pasted Layer

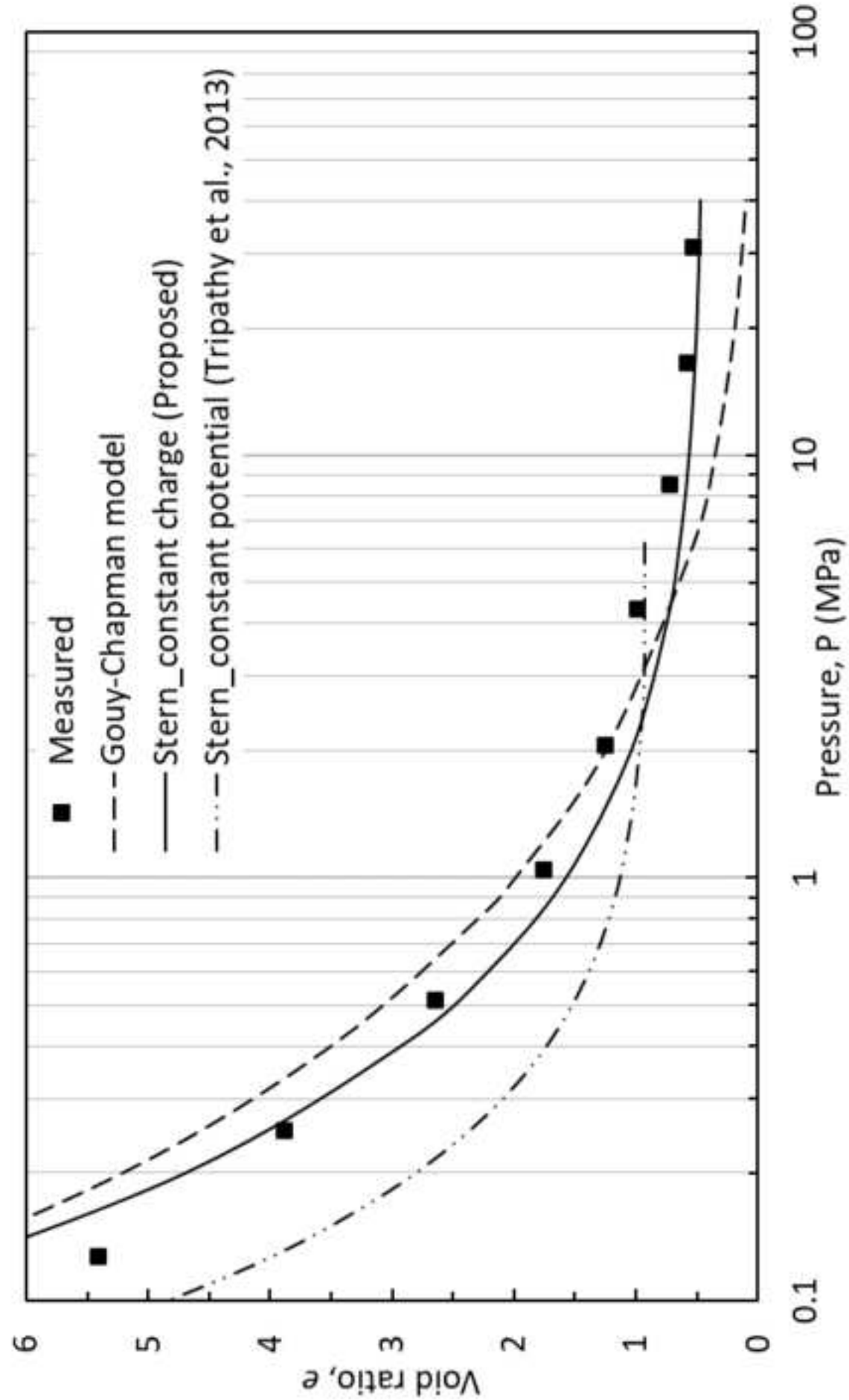

Fig.8a

Pasted Layer

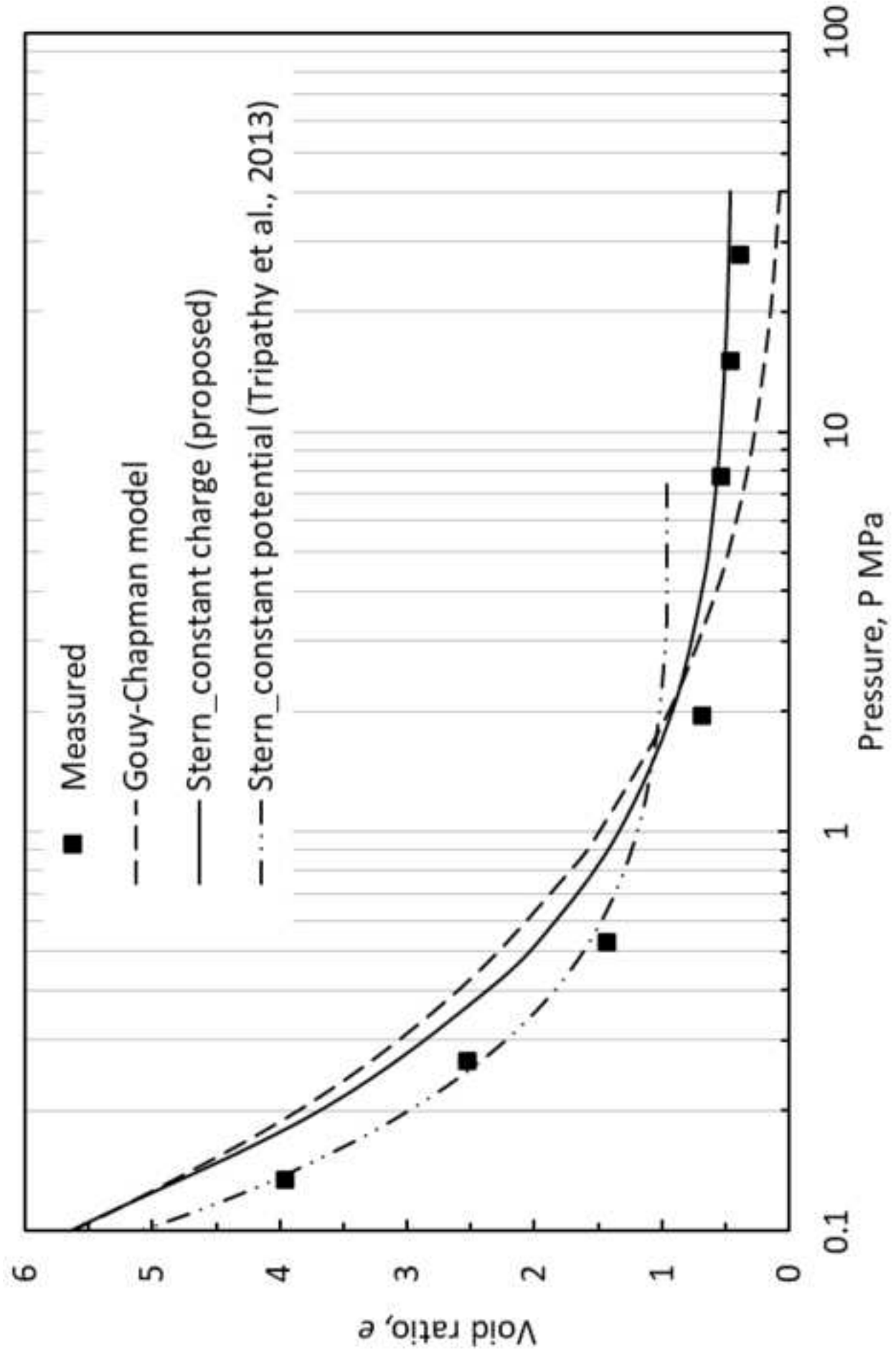

Fig.8b

Pasted Layer

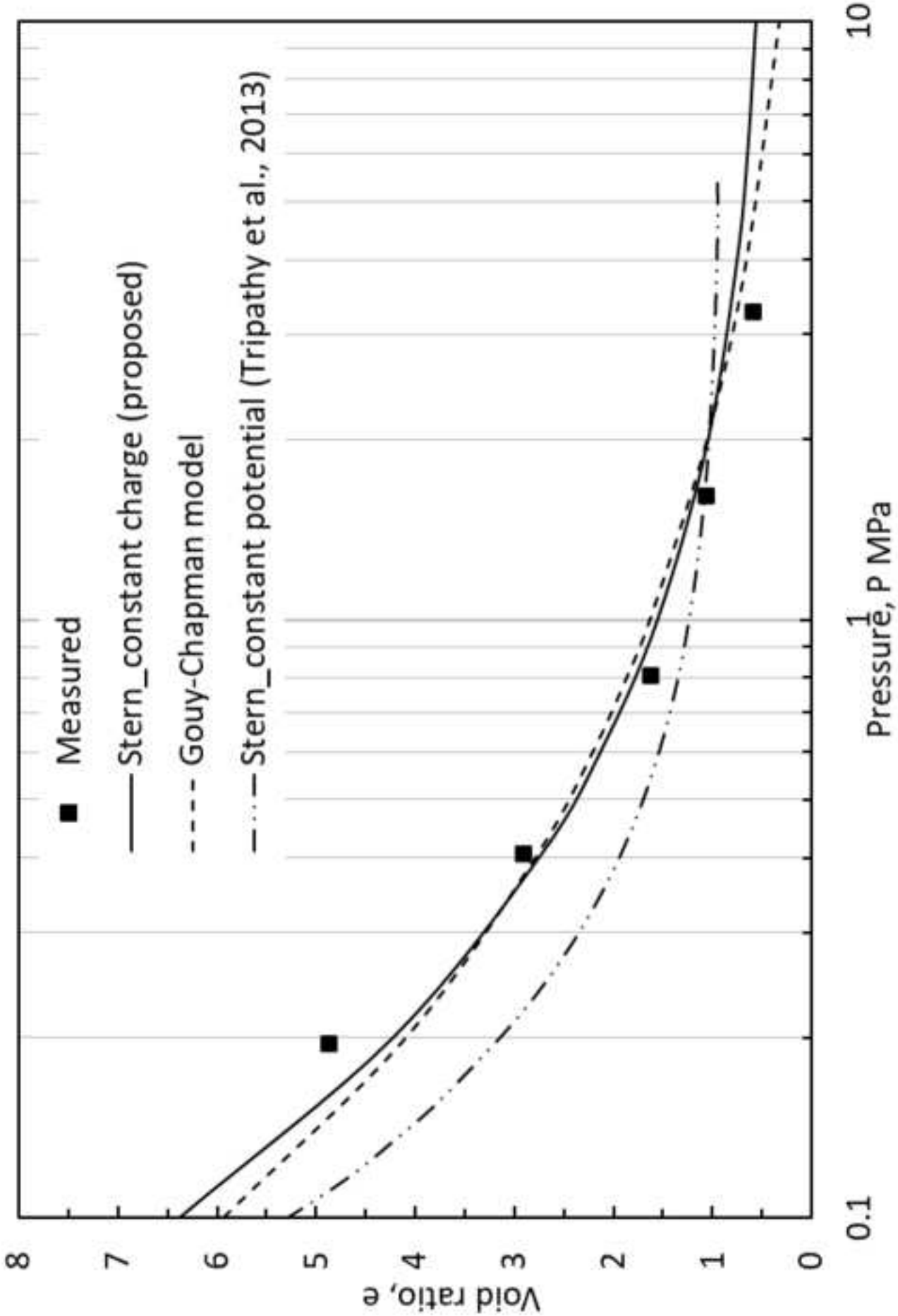

Fig.8c

Pasted Layer

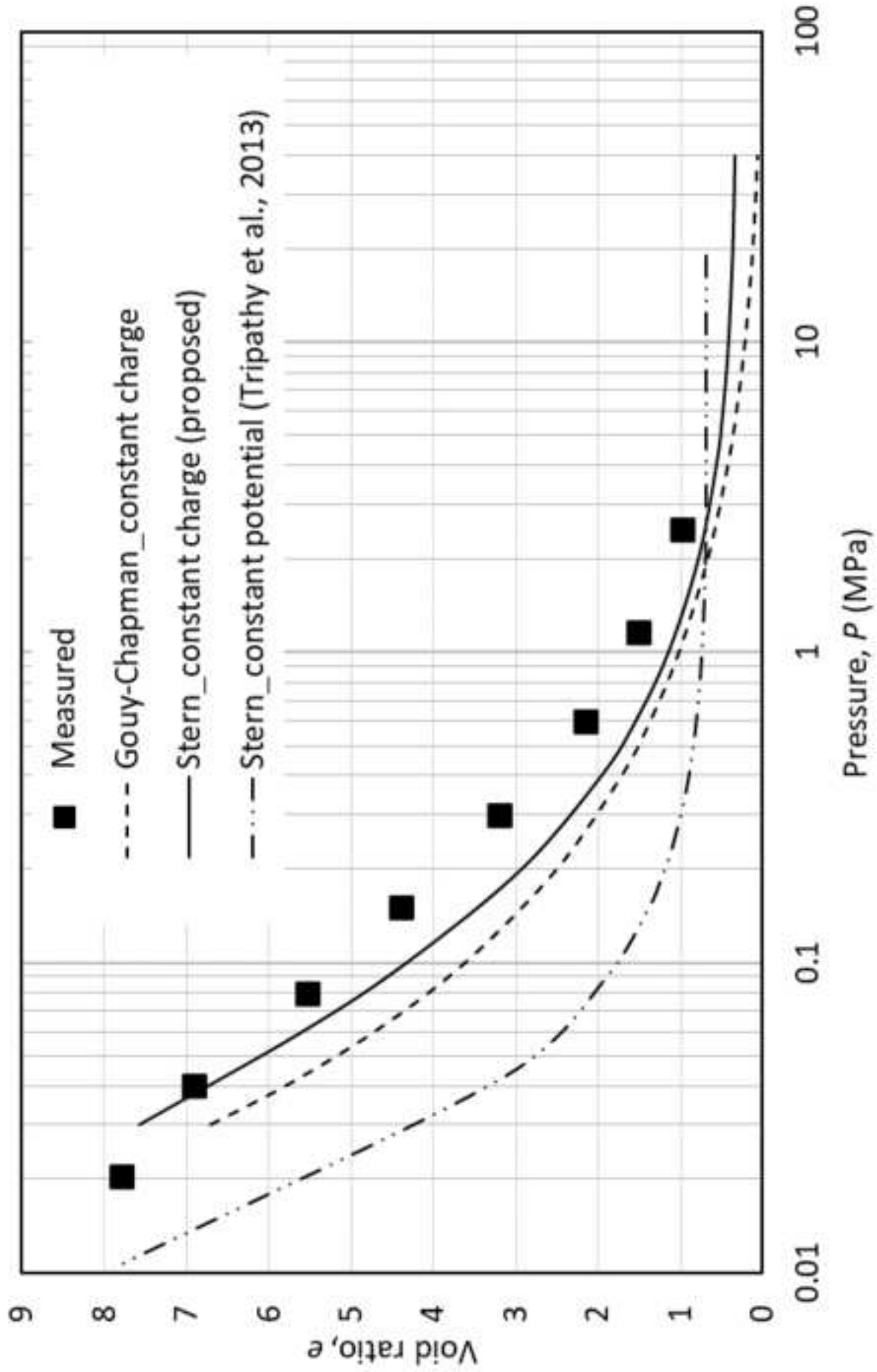

Fig.8d

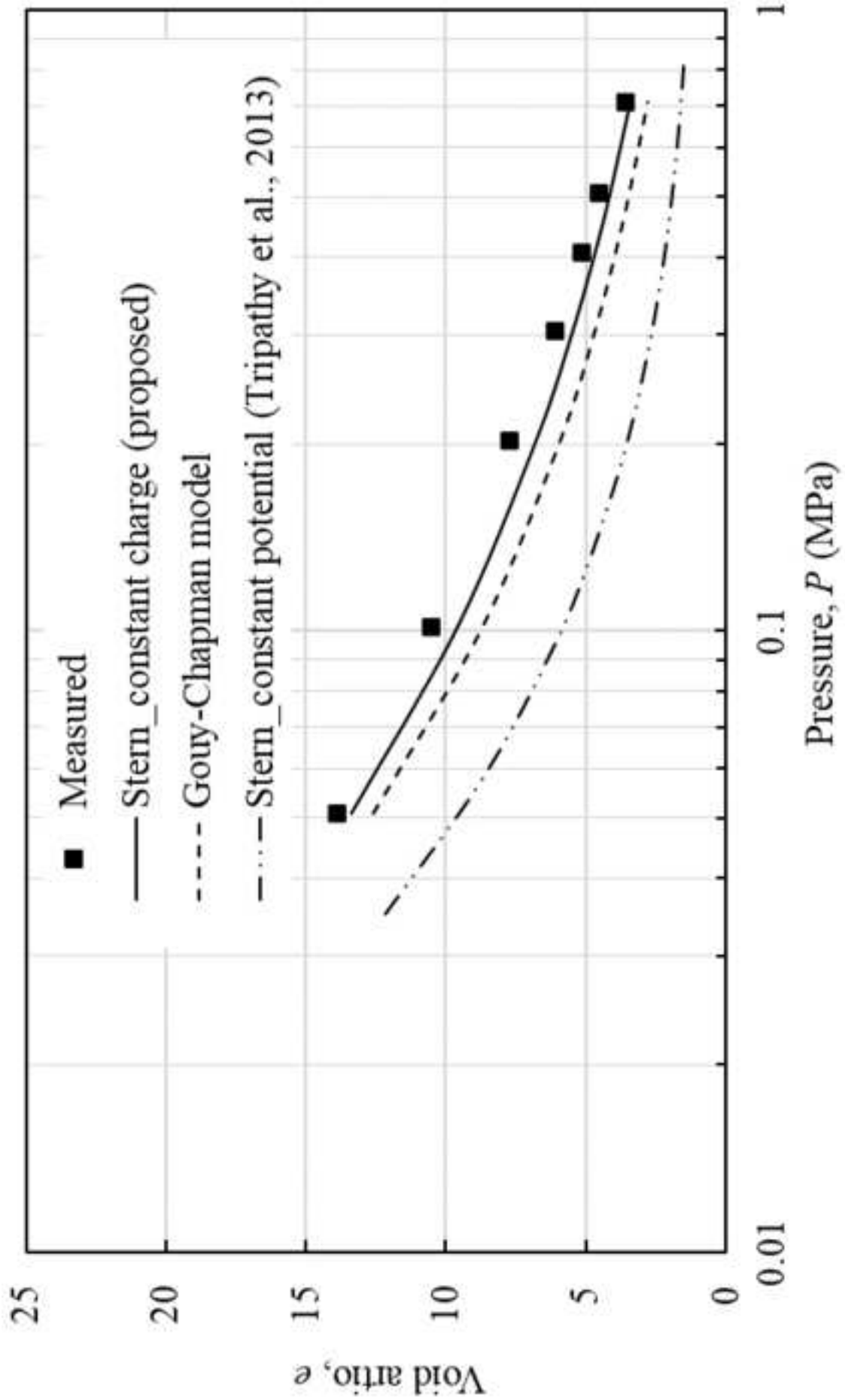

Fig.8e